DEVELOPMENT OF ZEOLITIC IMIDAZOLATE FRAMEWORKS FOR ENHANCING POST-COMBUSTION CO_2 CAPTURE

A Thesis

presented to

the Faculty of California Polytechnic State University,

San Luis Obispo

In Partial Fulfillment

of the Requirements for the Degree

Master of Science in Civil & Environmental Engineering

by

Dustin Lee

September 2020

© 2020

Dustin Lee

ALL RIGHTS RESERVED

COMMITTEE MEMBERSHIP

TITLE:	Development of Zeolitic Imidazolate Frameworks for Enhancing CO_2 Sorption Capacity for Post-Combustion Carbon Capture
AUTHOR:	Dustin Lee
DATE SUBMITTED:	September 2020
COMMITTEE CHAIR:	Amro El Badawy, Ph.D. Assistant Professor of Civil and Environmental Engineering
COMMITTEE MEMBER:	Tryg Lundquist, Ph.D., PE Professor of Civil and Environmental Engineering
COMMITTEE MEMBER:	Trevor Harding, Ph.D. Professor of Materials Engineering

ABSTRACT

Development of Zeolitic Imidazolate Frameworks with Enhancing CO_2 Sorption Capacity for Post-Combustion Carbon Capture

Dustin Lee

Post-combustion CO_2 capture is a promising approach for complementing other strategies to mitigate climate change. Liquid absorption is currently used to capture CO_2 from post-combustion flue gases. However, the high energy cost required to regenerate the liquid absorbents is a major drawback for this process. As a result, solid sorbents have been investigated extensively in recent years as alternative media to capture CO_2 from flue gases. For example, metal organic frameworks (MOFs) are nanoporous materials that have high surface areas, large pore volumes, and flexible designs. A large number of MOFs, however, suffer from 1) low CO_2 adsorption capacity at low pressure, which is the typical condition for flue gases, 2) degradation upon exposure to water present in flue gases, and 3) low selectivity of CO_2 when present in a mixture of gases. Zeolitic Imidazolate Frameworks (ZIFs) are heavily investigated MOFs for CO_2 sorption applications because they have better selectivity for CO_2 compared to other MOFs and are resistant to degradation in water due to their hydrophobic nature. However, ZIFs (e.g., ZIF-8) investigated for CO_2 sorption applications are typically produced using toxic solvents and their CO_2 sorption capacity is drastically lower than other types of MOFs. Post-synthesis modifications with amine functional groups have been known to increase CO_2 sorption capacity and selectivity within nanoporous materials. For ZIFs, previous research showed that sufficient loading with linear polyethyleneimine increased their CO_2 sorption capacity. Therefore, the objectives of this research were to a) investigate the CO_2 sorption capacity of ZIF-8 synthesized by solvothermal methods that use more

eco-friendly solvents (e.g., methanol and water) and b) introduce post-synthetic modifications to ZIF-8 using branched polyethyleneimine (bPEI) to enhance its sorption capacity. A custom quartz crystal microbalance (QCM) system was assembled and used to measure the CO_2 sorption capacity of unmodified and bPEI-modified ZIF-8 sorbent. The tests were conducted at 0.3 - 1 bar. The results showed that the unmodified ZIF-8 synthesized in methanol (ZIF-8-MeOH) had comparable crystal structure, thermal stability, surface area, and chemical properties to that of literature (Ta et.al 2018). ZIF-8-MeOH had a surface area of 1300 m^2/g and a CO_2 sorption capacity of 0.85 mmol CO_2/g ZIF-8 @ 1 bar. This surface area and sorption capacity are comparable to those of ZIF-8 made in dimethylformamide (DMF). Therefore, ZIF-8-MeOH proved to be a worthy candidate MOF for replacing the ZIF-8 made in DMF for CO_2 capture research. Water-based ZIF-8 was also synthesized in this study; however, its CO_2 sorption capacity was not tested because it exhibited a significantly lower surface area (732 m^2/g) compared to that of ZIF-8-MeOH. Modification of the ZIF-8-MeOH with bPEI resulted in a decrease in its CO_2 sorption capacity. This undesired outcome is likely a result of insufficient bPEI load (mass attached), on ZIF-8-MeOH (~ 10% w/w) combined with the surface area lost (~ 770 m^2/g) due to bPEI blocking some of the ZIF-8-MeOH pores. Therefore, the bPEI load attained in this study was not enough to compensate for the loss of surface area of the modified ZIF-8 and thus, the CO_2 sorption capacity decreased. Future investigations should enhance the post-synthetic modification by increasing the loading of amine functional groups onto the eco-friendlier ZIF-8-MeOH used in this study.

Keywords: Metal Organic Frameworks, Zif-8, Amine Functionalization, Carbon Capture, Quartz Crystal Microbalance

ACKNOWLEDGMENTS

I would like to express my gratitude to my advisor, Dr. Amro El Badawy, for his expertise, support, and encouraging words during graduate school. He has taught me much about the research process and I have learned valuable lessons that I will carry with me in my career.

I would also like to thank my committee members, Dr. Tryg Lundquist and Dr. Trevor Harding. Dr. Tryg Lundquist has provided much guidance in regards to career, life skills, and a new-found self-confidence. Dr. Trevor Harding has provided much insight into the field of materials engineering and has provided me access to all the tools to perform the material characterization work needed to complete my thesis.

I would also like to thank the Dr. John Hagen and Christopher Tusan from the Chemistry Department at Cal Poly for helping with the BET analysis. I would like to thank students Giannina Yu, Justin Ting, and Kyle Yue from the Materials Engineering Department for assisting me with the materials characterization and Dr. Yong Hao for teaching me all about materials characterization and serving on my committee for a short period before leaving Cal Poly. I would also like to thank Eric Beaton for being accommodating and providing access to the necessary materials engineering equipment.

I would like to thank my colleagues, friends, and family who have provided words of encouragement during these trying times.

Lastly, I would like to thank Cal Poly Interdisciplinary Projects Program (CPConnect) for giving me the opportunity to interact with different individuals from various disciplines and for providing funding to build the testing apparatus and purchase chemicals needed to carry out this research.

TABLE OF CONTENTS

Page

LIST OF TABLES

Table Page

LIST OF FIGURES

Figure Page

1. INTRODUCTION

Climate change is regarded as one of the greatest challenges of today's era, which has motivated development of many different pathways to mitigate it. The most prominent pathway is the development and use of renewable energy sources, which allows for low CO_2 emissions. However, with the continual increases in energy demand worldwide, more mitigation options, including carbon capture, are needed to curb the drastic consequences expected if net zero CO_2 emissions are not achieved by 2050 (IPCC, 2018).

Innovative technologies that aim to capture CO_2 emitted from point and non-point sources have been developed, these include post-combustion capture, pre-combustion capture, oxy-fuel combustion capture, and direct air capture. The most matured and most promising one is the post-combustion capture due to its feasibility of being implemented into existing coal-fired plants (Songolzadeh et al. 2014).

Post-combustion capture currently utilizes amine scrubbing, which exploits the high affinity that liquid amines have for CO_2 (Dutcher, Fan, and Russell 2015). This CO_2 absorption process has high energy costs associated with the regeneration of the liquid sorbents (Dutcher, Fan, and Russell 2015). Thus, solid sorbents have been investigated as a more energy efficient media for CO_2 capture (Samanta et al. 2012).

The most promising solid sorbents are nanoporous materials such as zeolites, carbonaceous materials, mesoporous silica, and metal organic frameworks (Samanta et al. 2012). Although all of these nanoporous sorbents have relatively high CO_2 adsorption capabilities, they suffer from disadvantages such as degradation in water vapor, low CO_2 selectivity, and low adsorption at flue gas conditions (Samanta et al. 2012). Metal organic frameworks (MOFs) present a pathway to overcome these challenges because of the ability to tune their structural characteristics through variations in synthesis

methods and conditions, choice of their building blocks, and introduction of post-synthesis modifications (Ding et al. 2018).

One particular class of MOFs that match the characteristics needed to adsorb CO_2 under flue gas conditions are zeolitic imidazolate frameworks (ZIFs). They have excellent mechanical, thermal, and chemical stability, high selectivity for CO_2, strong hydrophobicity, high surface area, comparable pore diameters to the size of CO_2 molecules, and large pore volumes (Park et al. 2006). One ZIF that has been heavily researched for CO_2 sorption is ZIF-8. The research on ZIF-8 has been focused on improving its CO_2 sorption capacity and selectivity. For example, Xian et al. (2015) functionalized ZIF-8 with linear polyethyleneimine and observed an increase in the CO_2 adsorption capacity to 1.3 mmol/g compared to 0.75 mmol/g for unmodified ZIF-8 at atmospheric pressure. However, this improved sorption capacity is still substantially lower than that for other types of MOFs. For example, Caskey et al. (2008) reported a CO_2 sorption capacity of 8 mmol/g for Mg-MOF-74. However, Mg-MOF-74 is not as stable in the presence of water and is not as selective for CO_2 as ZIF-8. Therefore, more research is needed to increase the sorption capacity of ZIF-8, that is highly stable in flue gas conditions, to exceed those of other types of MOFs.

The current research study capitalizes on the work performed by Xian et al. (2015) to optimize and increase the performance of ZIF-8 for sorption of CO_2. This thesis investigated the use of branched PEI rather than linear PEI as a modification agent for ZIF-8. Furthermore, the ZIF-8 used in this research was synthesized using more eco-friendly solvents (water and methanol) compared to the more toxic dimethylformamide (DMF) solvent used in the study by Xian et al. (2015). The key differences between linear PEI used by Xian et al. (2015) and the branched PEI used herein is that linear PEI is linear in structure and only contains secondary amines (Figure 1). On the other

hand, branched PEI contains primary, secondary and tertiary amine groups and has a branched structure (Figure 1). Considering primary and secondary amines react differently with CO_2 compared to tertiary amines, it was hypothesized that the presences of the various types of amine groups on the branched PEI molecule would enhance the CO_2 adsorption capacity of ZIF-8. Tertiary amines only react with CO_2 in humid conditions and thus could mean that branched PEI will be beneficial for CO_2 capture from humid flue gases. Furthermore, branched PEI was hypothesized to improve CO_2 capture compared to linear PEI because it is more effective in lowering the available pore volume in ZIF-8. This reduction in pore volume can cause an increase in van der Waals contacts between CO_2 and the ZIF-8 framework and thus, enhance CO_2 capture.

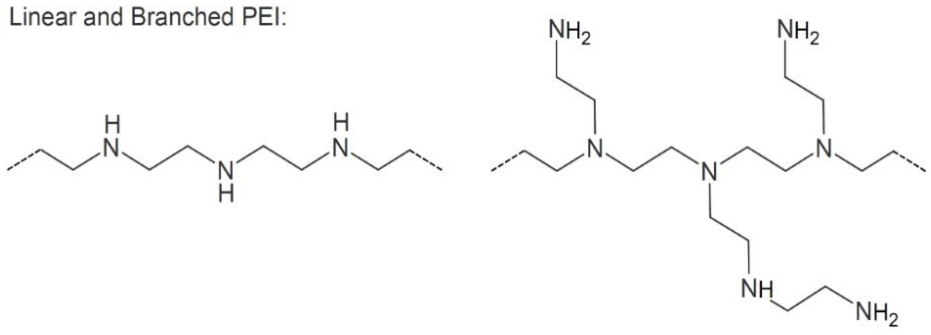

Figure 1. Linear and branched PEI (reproduced from polymerdatabase.com)

In addition to the ZIF-8 improvement goals mentioned above, the feasibility of using more eco-friendly ZIF-8 powders for CO_2 capture was investigated. Synthesis of ZIF-8 used in CO_2 sorption studies usually involved the use of harmful solvents such as DMF. The resulting ZIF-8 powders typically exhibited high surface areas and thus, were desirable for CO_2 sorption applications. However, other solvents, such as water and methanol, can be utilized to produce ZIF-8 with as a high quality as the ones produced using DMF (Jian et al. 2015; Ta et al. 2018). Such ZIF-8 powders have never been

tested for CO_2 capture. Therefore, the current study investigated the CO_2 adsorption capacity of ZIF-8 powders made using more eco-friendly solvents to allow for a more responsible and sustainable development of this technology.

1.1 Research Objectives

The main objectives of this research were to 1) develop a more eco-friendly ZIF-8 that possesses CO_2 adsorption capacity comparable to (or higher than) those of ZIF-8 made with DMF and 2) introduce post-synthesis modifications using branched polyethyleneimine (bPEI) to enhance the sorption capacity of the more eco-friendly ZIF-8 produced in the first stage of this research.

1.2 Hypotheses

1) ZIF-8 synthesized in methanol (MeOH) or water will result in CO_2 adsorption capacity comparable to (or higher than) that of ZIF-8 synthesized in DMF.
2) Modification of ZIF-8 (made in methanol or water) with bPEI will enhance its CO_2 sorption capacity.

1.3 Research Tasks

1) *Synthesis of ZIF-8:* ZIF-8 powders were synthesized in methanol and in water using published methods with slight modifications to optimize the properties of the product.
2) *Post-synthesis modification of ZIF-8:* the ZIF-8 produced in Task 1 was modified with bPEI using a wet impregnation method described in Chapter 3.
3) *Characterization of ZIF-8 powders:* both the unmodified and modified ZIF-8 powders were characterized using four analytical tools to verify the formation of ZIF-8, confirm the modification of ZIF-8 with amine groups, and determine the crystal structure, surface area, and percent branched PEI loaded into ZIF-8.

4) *Determination of CO_2 sorption capacity of ZIF-8:* a gravimetric method based on the use of a quartz crystal microbalance (QCM) was designed and assembled to quantify the sorption capacity of CO_2 on ZIF-8, unmodified and modified with branched PEI under pressure conditions representative of flue gas from post-combustion processes (i.e., 0.3-1 bar).

2. LITERATURE REVIEW

2.1 Climate Change

In 2018, the Intergovernmental Panel on Climate Change (IPCC) published a special report on the consequences of Global Warming of 1.5°C above pre-industrial levels(Masson-Delmotte et al. 2019). The report emphasized the increased need to develop solutions to combat climate change, or else there will be drastic consequences. Examples of the effects of climate change include ocean acidification; changing weather patterns; changes to coral reefs, forests, biological systems and low-lying coasts; and impacts on agricultural production (Hoegh-Guldberg et al. 2019). The IPCC special report indicated that limiting warming to 1.5°C above pre-industrial levels is the threshold to prevent catastrophic effects of climate change. The report also emphasized that a global net-zero CO_2 emissions must be achieved by 2050 to limit warming to the 1.5°C mark. The IPCC indicated that reduction in warming will require innovative technologies, renewable energy development, reduced deforestation, more sustainable agricultural methods, and changes in individual and group behavior.

The International Energy Agency (IEA)'s 2018 report on the global energy and CO_2 status showed that renewable energy growth increased from 6% in 2017 to 7% in 2018. The report also showed that renewable energy supplied about 45% of the total new electricity demand in 2018 as shown in Figure 1 (Energy Agency 2018). However, the global fossil fuels use has also increased, specifically natural gas and coal, to meet new electricity needs and thus, carbon dioxide emissions increased. Figure 3 shows that fossil fuels still account for 64% of the total electricity supply and their use continues to grow. The increasing trend in CO_2 emissions from combustion of fossil fuel shown in Figure 4 may indicate that the goal of achieving net zero CO_2 emissions by 2050 may not be attainable by only relying on renewable energy alone. Thus, the IPCC has also

suggested that the use of carbon capture technology will need to be coupled with other methods to attain this ambitious goal.

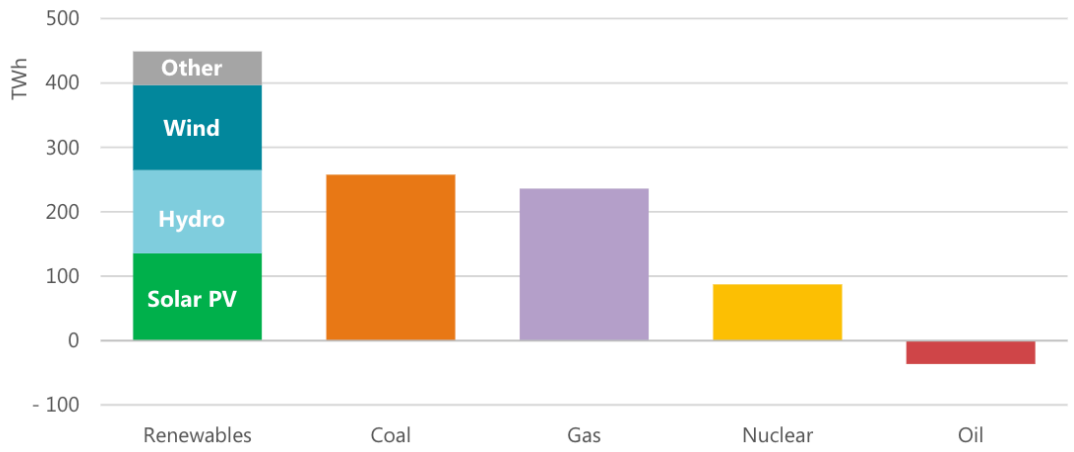

Figure 2. New electricity generated in 2017-2018 (IEA, Global Energy & CO2 Status Report: The latest trends in energy and emissions in 2018)

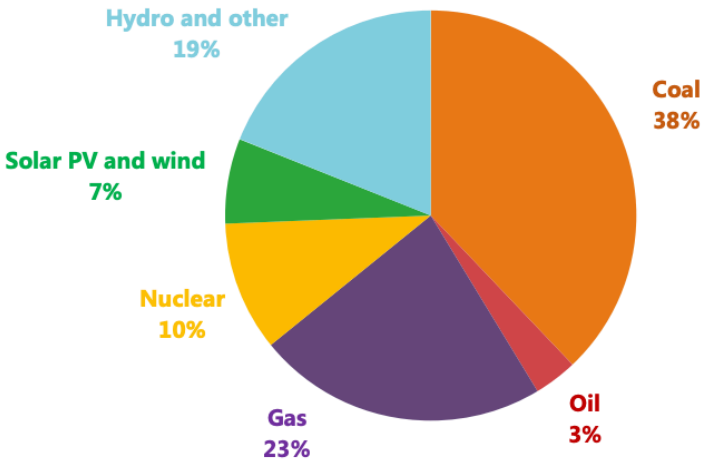

Figure 3. Energy generation mix, 2018 (IEA, Global Energy & CO_2 Status Report: The latest trends in energy and emissions in 2018)

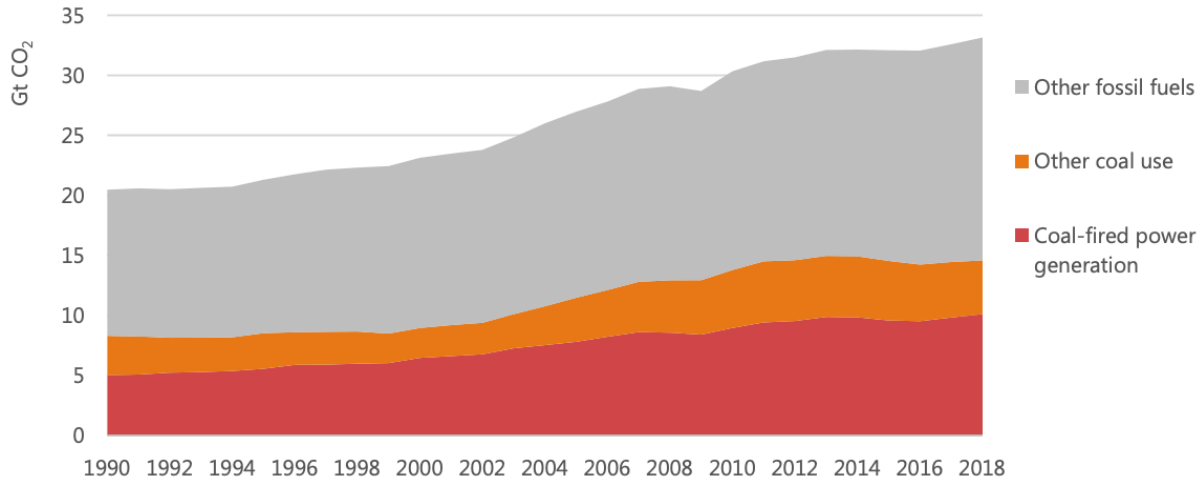

Figure 4. Global energy-related carbon dioxide emissions by source (Global Energy & CO_2 Status Report: The latest trends in energy and emissions in 2018)

2.2 Current Technology for Carbon Capture

Current technologies for carbon capture are split into four categories: pre-combustion capture, oxy-fuel combustion capture, post-combustion capture, and direct air capture (removal of CO_2 from ambient air (Koytsoumpa, Bergins, and Kakaras 2018). These carbon capture categories focus on capturing CO_2 emissions resulting from the combustion of from natural gas and coal, which generate 61% of the electricity worldwide.

Pre-combustion capture, shown in Figure 5, involves reacting a fuel with oxygen, air, or steam to produce a synthesis gas, syngas, which is composed of carbon monoxide and hydrogen (Jansen et al. 2015). This gas is then sent along with steam to a catalytic converter to turn the carbon monoxide into carbon dioxide and hydrogen. The carbon dioxide exiting the catalytic converter is captured by a chemical or physical absorption process, which lead to the production of a hydrogen rich fuel. Pre-combustion carbon capture has the advantage of producing a high purity fuel as well as CO_2 at elevated

pressures and higher concentrations. These attributes would reduce transportation costs and ability for a power plant to switch between hydrogen production and electricity generation (Jansen et al. 2015). Nevertheless, pre-combustion capture is not as widely used as post-combustion capture due to the high capital costs associated with syngas generation as well as the efficiency losses during a) syngas production (6% efficiency loss), b) CO_2/H_2 separation (5% efficiency loss), c) water-gas shift (3-3.5% efficiency loss), and d) compression and drying (2% efficiency loss) (Jansen et al. 2015).

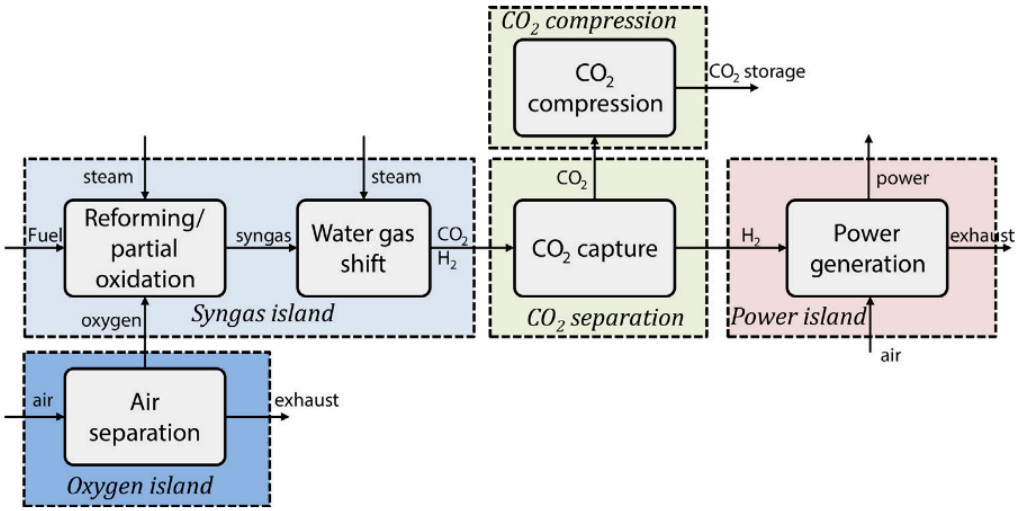

Figure 5. Pre-combustion capture for power generation (reproduced from (Jansen et al. 2015)

Oxy-fuel combustion capture involves the separation of oxygen from air and use of that oxygen to combust the fuel of choice. A schematic of the process is presented in Figure 6. This process produces a smaller volume of flue gas, thus increases the CO_2 concentration up to 90% (Sanz-Pérez et al. 2016). The CO_2 rich gas produced is usually wet and so needs to be condensed and purified to remove impurities using physical and chemical absorption processes (Kanniche et al. 2010). However, the oxy-fuel combustion is not widely used due to the high cost of separating oxygen from air.

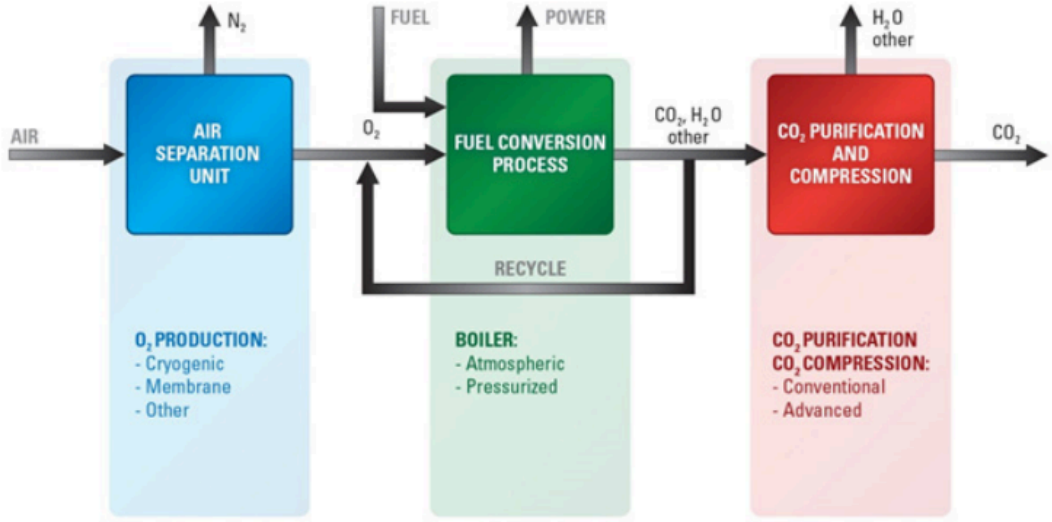

Figure 6. Oxy-fuel combustion process (reproduced from U.S. Department of Energy, (Changing Role of Natural Gas in Energy Generation n.d.)

Post combustion capture is the CO_2 removal from flue gases, which happens after combustion of the fuel. The flue gas usually consists of a relatively small concentration of CO_2 (13-15%) and the rest of the gas components includes particulate matter, water vapor, NO_x, and SO_x (Wang et al. 2017). The flue gas typically has relatively high temperatures ranging from 100°C to 150°C (Songolzadeh et al. 2014). Various methods can be used to separate the CO_2 from the flue gas as shown in Figure 7. Of these methods, chemical absorption through amine solvents is the most commonly used technology for removal of CO_2 under the flue gas conditions; however, it is an energy intensive process (Koytsoumpa, Bergins, and Kakaras 2018). Post-combustion capture is as an attractive CO_2 capture technology due to its lower capital costs compared to pre-combustion capture and the ability to install it at current plants burning fossil fuel (Songolzadeh et al. 2014).

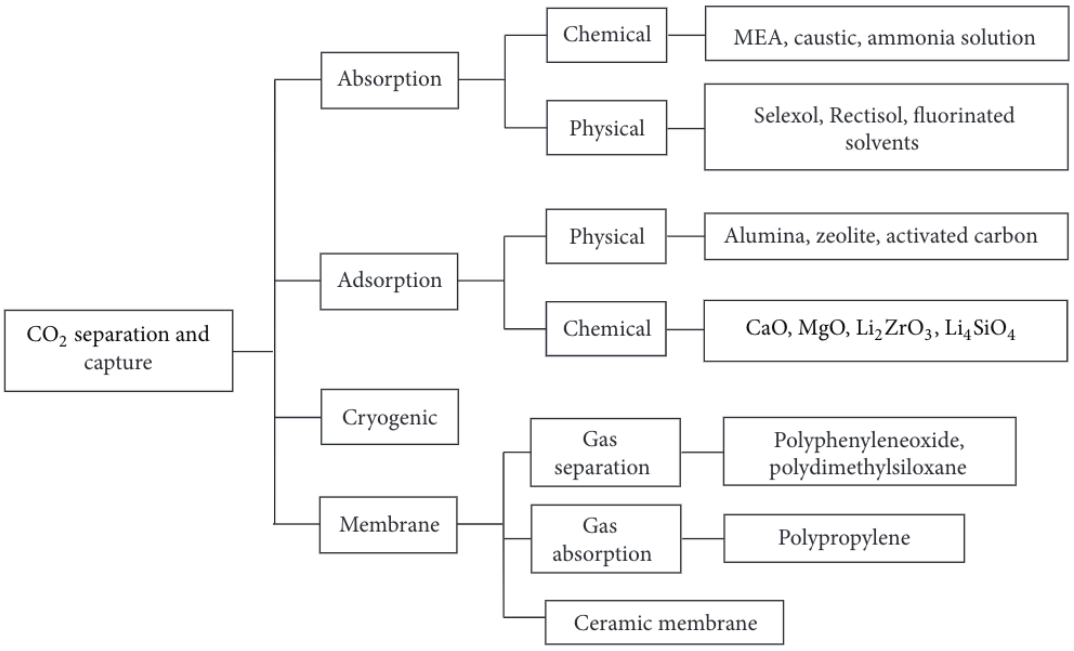

Figure 7. Post-combustion pathways for CO2 removal (reproduced from (Songolzadeh et al. 2014)

Unlike the aforementioned categories that capture carbon dioxide from a point source, direct air capture is the capture of CO_2 from ambient air. This method has many advantages that include capturing emissions from non-point and point sources, can be placed anywhere, and is not tampered with high concentrations of contaminants present in flue gases (Sanz-Pérez et al. 2016). Because approximately half of the CO_2 emissions come from non-point sources, this method should be used in conjunction with the other aforementioned capture approaches in order to combat climate change (Sanz-Pérez et al. 2016). Membranes, chemical and physical sorbents, electrochemical approaches, photocatalytic conversion, and mineral carbonation methods have been suggested for direct carbon capture. However, chemical sorbent materials produced the best results for carbon capture due to the low concentration of CO_2 (~ 400 ppmv) present in ambient air (Sanz-Pérez et al. 2016).

Of all the carbon capture methods, post-combustion carbon capture is the most mature and flexible because it can be installed at existing coal and natural gas plants (Songolzadeh et al. 2014). The current technology being used to separate CO_2 from flue gas is known as amine scrubbing and it relies on the use of four classes of aqueous liquid sorbents: carbonate, tertiary amines, secondary amines, and primary amines (Rochelle 2016).These aqueous liquid sorbents are usually contained in an absorption column as shown in Figure 8 and operated in a counter flow mode against the flue gas. The spent liquid sorbent that absorbs the CO_2, also known as rich-loaded solution, is then pumped to a stripper where it flows against a stripping steam. The stripping steam desorbs the CO_2 from the liquid absorbent and compresses the CO_2 gas to be stored or shipped elsewhere. The now stripped liquid sorbent, or lean solution, is sent back to the absorber to be re-used. The main disadvantage of this process is the high energy cost of regenerating the sorbent media, current commercial processes require 2.6 GJ of energy for each metric ton of CO_2 captured (Koytsoumpa, Bergins, and Kakaras 2018).

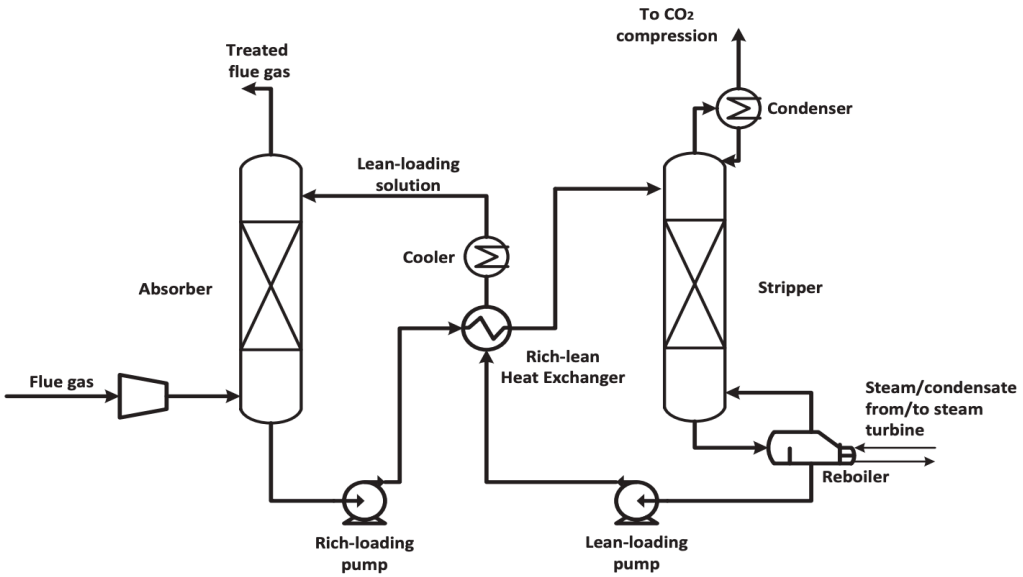

Figure 8. Common chemical absorption process for CO2 capture (reproduced from (Wang et al. 2017)

To combat the high cost of operation, other technologies are being developed such as adsorbing CO_2 using solid sorbents. Adsorption has the advantage of reduced energy for regeneration as well as greater CO_2 sorption capacity and CO_2 selectivity (Samanta et al. 2012). The criteria for choosing an optimal solid sorbent includes its CO_2 adsorption capacity, selectivity for CO_2 over other compounds in the flue gas, rapid CO_2 adsorption and desorption kinetics, cost, mechanical and chemical stability, and ease of regeneration (Samanta et al. 2012).

Various types of solid sorbents have been studied including carbonaceous materials, zeolites, metal organic frameworks, and mesoporous silica (Sneddon, Greenaway, and Yiu 2014). These adsorbents tend to have a high surface area to volume ratio and high pore volume. In addition, the pore diameters tend to be in the nanoscale range as shown in Figure 9 and thus, such sorbents can be classified as nanoporous materials.

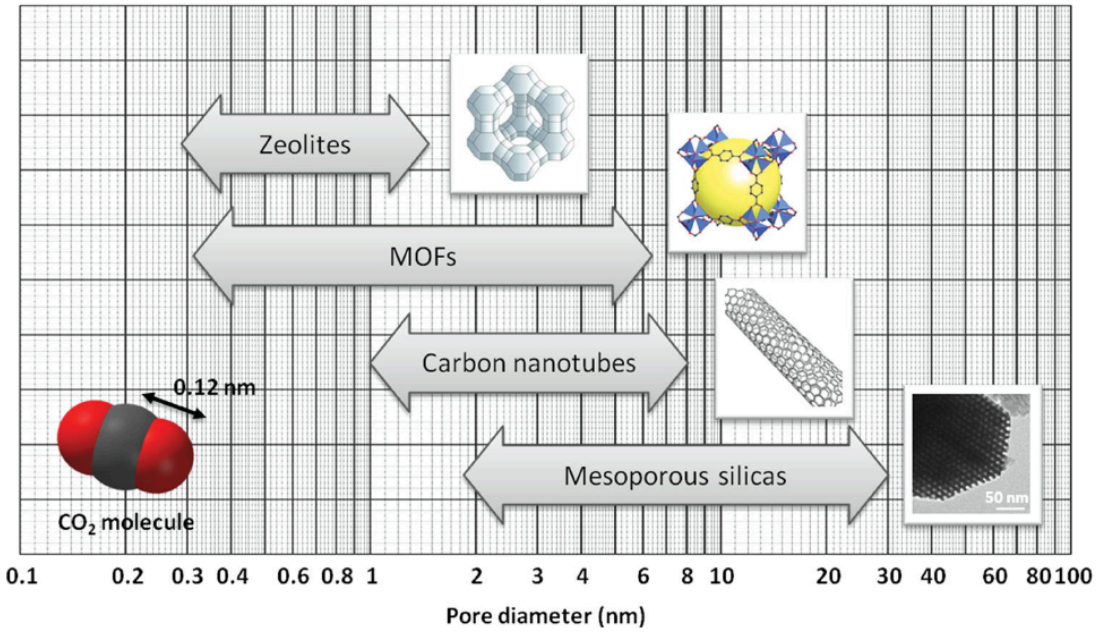

Figure 9. Structural characteristics of nanoporous sorbents (reproduced from (Sneddon, Greenaway, and Yiu 2014)

Zeolites are hydrated aluminosilicates with highly ordered structures (Sneddon, Greenaway, and Yiu 2014). These naturally occurring substances have been used in industry as adsorbents and catalysts. Zeolites have an especially high selectivity for CO_2 due to their pore diameter (0.4-0.5 nm) being comparable to the diameter of CO_2 molecules (0.31 nm). However, zeolites are not effective in post-combustion capture applications as they lose their CO_2 adsorption capacity because of the water and nitrogen present in the flue gas.

Nanoporous carbon-based adsorbents include activated carbon, carbon nanotubes, and carbon molecular sieves (Samanta et al. 2012). These materials are attractive for CO_2 sorption applications due to their relatively low cost as they can be found in natural forms such as bamboo (Samanta et al. 2012). The only exception being carbon nanotubes, but their cost may be compensated for by their higher selectivity for CO_2 compared to other carbon-based adsorbents (Samanta et al. 2012).

Mesoporous silica is a form of silica in which the pore sizes are highly uniform and it has high surface area (>1000 m^2/g), through the use of a template that the silica adheres to (Alothman 2012). Despite its high uniformity and surface area, mesoporous silica does not adsorb gases as readily as zeolites due to silica's larger pore size (> 2 nm) (Sneddon, Greenaway, and Yiu 2014). As a result, mesoporous silica is usually modified with amines in order to improve its ability to capture CO_2 through chemisorption (Sneddon, Greenaway, and Yiu 2014).

The most recent development in CO_2 solid adsorbents are the metal organic frameworks (MOFs). These materials have tunable structural characteristics and functions through functional groups, organic ligands, metal ions, and activation methods (Ghanbari, Abnisa, and Wan Daud 2020). Since MOFs are the focus of this thesis, more

discussions on their structure, properties and applications in CO_2 adsorption are provided in the next section (Section 2.3).

The advantages and disadvantages of each of the aforementioned CO_2 solid adsorbents are listed in Table 1. This table shows that metal organic frameworks are promising and with more research and development, the majority of their disadvantages may be overcome due to the high tunability of their structures and functions.

Table 1. Advantages and disadvantages of common adsorbents in post-combustion carbon capture (adapted from (Samanta et al. 2012)

Adsorbent	Advantages	Disadvantages
Zeolites	• Favorable Adsorption Kinetics • High adsorption capacity at mild operating conditions (0-100°C)	• Presence of impurities significantly impact performance • CO_2 can chemisorb onto surface, making pressure swing approach unviable
Nanoporous Carbon	• High thermal stability • Favorable adsorption kinetics • Raw material costs (except for carbon nanotubes) • Large adsorption capacities at elevated pressures • Pressure swing approach for desorption of CO_2	• Low CO_2 capacity at mild conditions • Wide variety of pore characteristics (except for carbon nanotubes) • Negatively impacted by NO_x, SO_x, and H_2O
Mesoporous Silica	• No use of toxic chemicals that Metal Organic Frameworks utilize • Tunability of pore size and volume using templates. • When modified with amines, minimally impacted by CO_2 partial pressure • When modified, humid environments improve adsorption efficiency	• Weak interaction between CO_2 at low pressures due to large pore size unless modified • Surface covered with mildly silanol groups • Removal of template requires use of solvent and emits CO_2

	• Favorable adsorption kinetics	
Metal Organic Frameworks	• High thermal stability • Adjustable chemical stability • Extra high porosity • High adsorption capacities at elevated pressures • Easily tunable pore characteristics	• Negatively impacted by NO_x, SO_x, and H_2O • Low selectivity in CO_2/N_2 gas streams • Lack of experimental data on performance after multiple adsorption/desorption cycles • Pressure and temperature swing approaches for desorption are not adequately researched

2.3 CO_2 Adsorption using Metal Organic Frameworks

Metal organic frameworks are a subclass of coordination polymers, which are polymer structures made up of coordination complexes. These coordination complexes are usually composed of a metal cation in the middle with ligands or other molecules linked to it as seen in Figure 2-9 (Ghanbari, Abnisa, and Wan Daud 2020). MOFs usually have three main attributes: permanent porosity, strong 3D structures, and modular design (Ghanbari, Abnisa, and Wan Daud 2020).

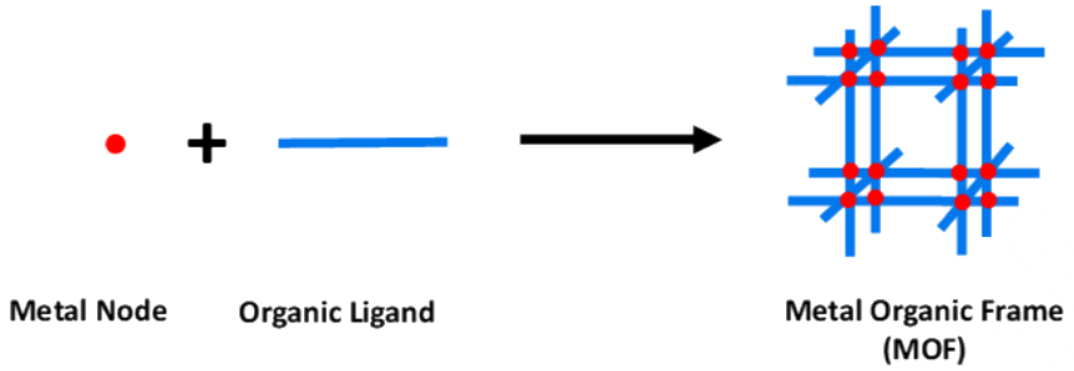

Figure 10. MOF formation (reproduced from (Ghanbari, Abnisa, and Wan Daud 2020)

Currently, 163,037 possible MOFs have been simulated in the Northwestern MOF database (Wilmer et al. 2012). CoRE MOF is another database that, as of 2019, has listed 14,000 MOFs that have been actually synthesized (Chung et al. 2019). The highest reported surface area for a MOF in the CoRE MOF database is 8318.18 m^2/g. Metal organic frameworks are currently applied in many fields such as extraction of antibiotics, removal of toxic pollution, gas adsorption, catalysis, electrochemical sensors, electrochemical charge storage, batteries, supercapacitors, fuel cells, and drug delivery systems (Safaei et al. 2019).

MOFs have unique properties that make them promising for CO_2 adsorption applications. The choice of ligand and metal cation for synthesis of MOFs dictate their pore size, pore volume, crystallinity, surface area, shape, and use of each MOF. Selection of these building blocks allows for better CO_2 adsorption, which occur according to the following interactions: open metal sites, Lewis basic sites, polar functional groups, CO_2 molecule and pore size interaction, framework flexibility, and hydrophobicity (Ding et al. 2018).

Open metal sites usually are formed on MOFs through the use of a terminal ligand such as water or organic solvents, which are removed at the end of the synthesis process through heat or vacuum. The removal of the ligand improves the porous structure of the MOFs as well as provides a Lewis acid site that coordinates with CO_2 (Ding et al. 2018). These open metal sites increase the CO_2 affinity of the MOFs.

The other building block of MOFs, the ligand, also aids in the CO_2 adsorption through Lewis basic sites, which is the CO_2 removal mechanism that conventional amine scrubbing relies on (Ding et al. 2018). Introduction of polar functional groups such as -OH, -COOH, and others can also increase the affinity for CO_2 due to the attraction between the polar functional groups and the quadrupole of the CO_2 molecule (Ding et al. 2018). A greater distribution of smaller pore sizes, pores around 0.3 nanometers, also known as micropores, allow for preferential adsorption of CO_2 by the MOFs over other gases such as N_2 (Ding et al. 2018). When choosing the organic linker, the MOF can also be changed to be become a more flexible instead of a rigid framework. Being a flexible framework allows higher selectivity for CO_2 due to a gate opening mechanism, which could be achieved through the use of polar functional groups (Ding et al. 2018).

Lastly, the hydrophobicity of MOFs is another desirable property that improves their CO_2 selectivity and sorption capacity. The flue gas streams typically contain water along with other gases and such components compete with CO_2 for the adsorption sites of MOFs. Therefore, hydrophobic metal organic frameworks have low affinity for adsorbing water. Table 2 provides examples of MOFs that have been developed for CO_2 sorption and their mechanism of work.

Table 2. Examples of MOFs developed for CO2 adsorption (adapted from (Ding et al. 2018)

MOF Type	**CO_2 Adsorption Capacity (mmol/g)**	**Temp (K)**	**Mechanisms of CO_2 adsorption**
Mg-MOF-74	8.0	296	Open Metal Sites
FJI-H14	6.5	298	Open Metal Sites and Lewis Basic Sites
bio-MOF-11	4.1	298	Lewis Basic Site
USTC-253-TFA	2.9	298	Polar Functionality
CPM-33b	5.6	298	Microporous
$(choline)_3[In_3(btc)_4]$ 2DMF	3.2	273	Micropores and Polar Functionality
CPM-5	2.4	299	Micropores and Open Metal Sites
PCN-123	1.0	295	Flexible Framework
ZIF-100	0.95	298	Microporous, Hydrophobic, Polar Functionality

As shown in Table 2, the CO_2 sorption capacity differs widely by the type of MOFs used with Mg-MOF-74 exhibiting the highest CO_2 sorption capacity. However, Mg-MOF-74 is hydrophilic and it degrades under flue gas conditions due to exposure to water vapor (Ghanbari, Abnisa, and Wan Daud 2020). In general, water vapor, which constitutes around 5-7% of the flue gas stream, and high temperatures are problematic for most MOFs except for a few types including a subclass of MOFs called zeolitic imidazolate frameworks (ZIFs) (Ghanbari, Abnisa, and Wan Daud 2020).

The synthesis method to create MOFs can enhance their CO_2 adsorption, by changing the surface area, crystallinity, and pore properties. Methods for synthesis of MOFs

include diffusion, hydro(solvo)thermal, microwave, electrochemical, mechanochemical, dry gel conversion, microfluidic synthesis, and sonochemistry (Safaei et al. 2019). Different synthesis parameters such as drying time, pH, reaction time, and the choice of solvent affect the properties of MOFs (Safaei et al. 2019) as shown in Figure 11.

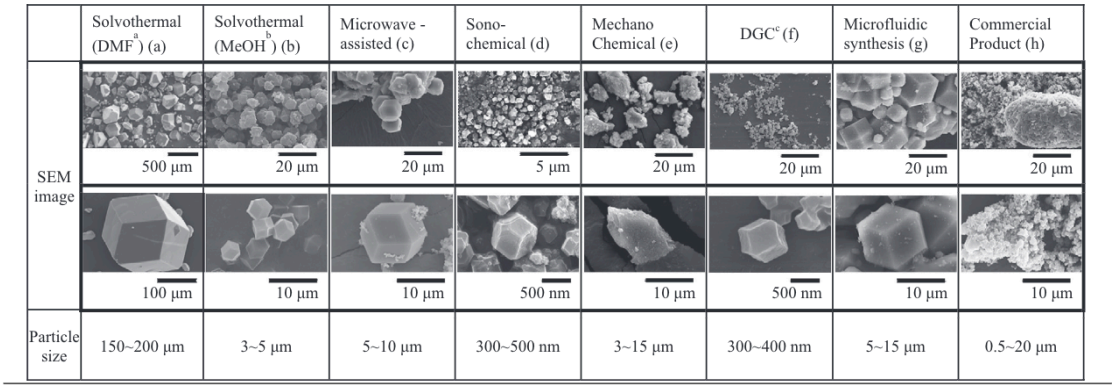

Figure 11. SEM images showing particle size and shape of ZIF-8 MOFs resulting from different synthesis methods (reproduced from (Lee et al. 2015)

Along with changing the synthesis methods and choice of precursors, altering the MOF after synthesis can also garner increased CO_2 adsorption, this is known as post-synthetic modification. Post-synthetic modification falls into two categories, post-synthetic modification (PSM) and MOF composites (Ding et al. 2018).

PSM includes the introduction of additional functional groups, exchange of metal ions, and modification of organic linkers (Ding et al. 2018) . The PSM process introduces functional groups including hydrazines and amines into a suitable MOF such as Mg_2(dobpdc) (Ding et al. 2018). Although this Mg_2(dobpdc) MOF had a reduced surface area and pore volume after the PSM process, it had an increased CO_2 adsorption capacity and selectivity (Ding et al. 2018). Exchanging of metal ions was observed when Zr(IV) ions of UiO-66 was replaced with Ti(IV) through an immersion of a $TiCl_4(THF)_2$ in

a dimethylformamide (DMF) solution. This modification resulted in an increased CO_2 adsorption capacity from 2.2 mmol/g to 4.0 mmol/g due to the reduction of the MOF's pore size. The reduction of pore size was attributed to Ti-O bonds being smaller than Zr-O bonds (Ding et al. 2018). The organic linker in Cr-MIL-101-SO_3H was modified with alkylamines to produce Cr-MIL-101-SO_3H-TAEA to increase its CO_2 adsorption capacity (Ding et al. 2018).

The second method of post synthesis modification, metal composites, is a more flexible approach. This post-synthesis modification can be applied to metal organic frameworks that have smaller pores, no functional groups on the linker, and no open metal sites. Composites have included small molecules, polymers, 2D structures, and 3D materials. Combining the MOF and the composite can lead to greater CO_2 adsorption capacities and enhanced stability (Ding et al. 2018).

2.4 ZIF MOFs for CO_2 Capture

As mentioned previously, zeolitic imidazolate frameworks (ZIFs) are a subclass of MOFs that have great potential for CO_2 capture because they can withstand the flue gas conditions (e.g., humidity and temperature). ZIFs combine the tunable porosity, structural flexibility, and functionalization potential of MOFs with the thermal and chemical stability of zeolites (Chen et al. 2014) . Furthermore, the structure of ZIFs are identical to zeolites, a four-corner sharing tetrahedra, which allows the formulations of hundreds of different ZIFs (Phan et al. 2010) as there are zeolites. A few examples of ZIF formulations are shown in Figure 12.

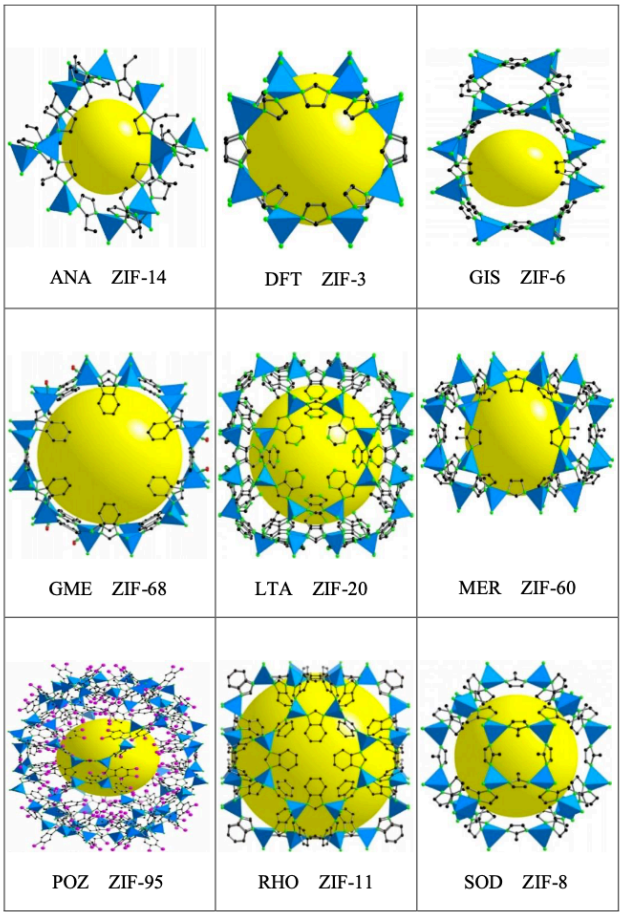

Figure 12. 3D structures of different types of ZIFs. Pore volume showed in yellow and blue tetrahedra are metal ions surrounded by organic linkers (Reproduced from Phan et al. 2010)

ZIFs are usually in the form of M-Im-M structure, where the M stands for a metal such as Zn and Im stands for the imidazolate linker (Phan et al. 2010). They have a thermal stability of up to 500°C and are highly stable in chemical and aqueous media as previously mentioned (Phan et al. 2010). Examples of ZIFs that have been tested for CO_2 sorption applications are presented in Table 3. This data shows that ZIFs differ greatly in pore sizes, adsorption capacities, and surface areas. Of these ZIFs, the most researched and commercialized one is the 8th synthesized ZIF, ZIF-8.

Table 3. Example ZIFs and their properties at 1 bar and varying temperatures (T)

ZIF	CO_2 adsorption capacity (mmol/g) at 1 bar	Surface Area (m^2/g)	Pore Size (nm)	Reference	T (K)
8	0.75	1150	3.4	Xian et al., 2015	298
68	1.68	1090	7.5	Phan et al., 2010	273
69	1.81	950	4.4	Phan et al., 2010	273
70	2.46	1730	13.1	Phan et al., 2010	273
78	2.30	620	3.8	Phan et al., 2010	273
79	1.61	810	4	Phan et al., 2010	273
81	1.71	760	3.9	Phan et al., 2010	273
82	2.35	1300	8.1	Phan et al., 2010	273
95	0.86	1050	3.7	Phan et al., 2010	273
100	1.46	595	3.4	Phan et al., 2010	273

ZIF-8 is formed using a zinc hydrated salt and 2-methlydimazole and can be prepared in a plethora of ways (Chen et al. 2014). As shown in Table 3, ZIF-8 has a relatively modest CO_2 adsorption capacity compared to the other MOFs. Despite this disadvantage, ZIF-8 has a relatively high surface area and is filled with micropores that may be functionalized with composites or other functional groups to enhance its sorption capacity.

The most notable functional groups used in post-synthesis modification of ZIF-8 are amines due to their affinity for CO_2 (Rochelle 2016). Specifically, primary and secondary amino groups in the form of R_2NH or RNH_2 react with CO_2 to form a carbamate, R_2NHCOO^-, as shown in Equation 2-1 (Rochelle 2016) These reactions are relatively fast (Rochelle 2016). Tertiary amino groups (R_3N) also have affinity for CO_2 but their reactions are slow and only react with CO_2 in the presence of water shown in Equation 2-2.

$$2R_2NH + CO_2 \rightarrow R_2NHCOO^- + R_2NH_2^+$$

Equation 2-1: Primary and Secondary Amine Reaction with CO_2

$$R_3N + H_2O + CO_2 \leftrightarrow R_3NH^+ + HCO_3^-$$

Equation 2-2: Tertiary Amine Reaction with CO_2

These amine compounds have been successfully deposited onto MOFs to improve their CO_2 sorption capacity and selectivity as shown in the examples in Table 4. It is noted that the amine compounds in Figure 2-12 have been also used as liquid absorbents for amine scrubbing of CO_2.

Name	Structure	Name	Structure
Amines		Silanes	
Monoethanolamine (MEA)		3-aminopropyltrimethoxysilane (APTS)	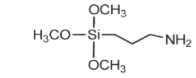
Diethanolamine (DEA)	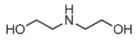	3-aminopropyltriethoxysilane (APTES)	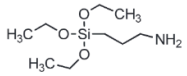
Triethanolamine (TEA)	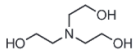	N-[3-(trimethoxysilyl)propyl]-ethylenediamine (AEAPTS)	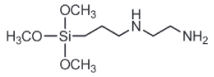
Polyethyleneimine (PEI)	 (R=H for linear, R=H or CHx for branched)	N-[3-(trimethoxysilyl)propyl]-diethylenetriamine (DAEAPTS)	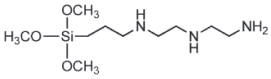
Diethylenetriamine (DETA)	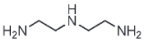	Ethylhydroxyl-aminopropyl-trimethoxyslane (EHAPTS)	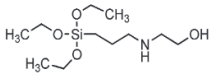
Tetraethylenepentamine (TEPA)	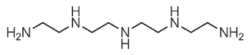	Diethylhydroxyl-aminopropyl-trimethoxyslane (DEHAPTS)	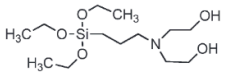
		Cyclic	
Tetraethylenepentamine-acrylonitrile (TEPAN)	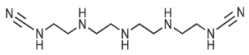	Aziridine	
Pentaethylenehexamine (PEHA)	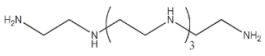	1,8-diazabicyclo[5.4.0]undec-7-ene (DBU)	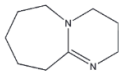
2-Amino-2-methyl-1,3-propanediol (AMPD)	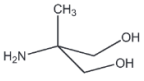	1,5-diazobicyclo [4.3.0]non-5-ene (DBN)	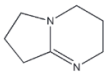
2-(2-Aminoethylamino)ethanol (AEAE)	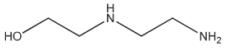	N-methyltetrahydropyrimidine (MTHP)	

Figure 13. Structures of widely used amines for sorbent functionalization (reproduced from Samanta et al. 2012)

Table 4. Solid sorbents functionalized with amines (reproduced from (Dutcher, Fan, and Russell 2015)

support	amine	equilibrium capacity (mmol/g)	CO_2 partial pressure (bar)	temp (°C)
mesoporous carbon	PEI	4.7	1	30
mesoporous silica	TEPA	4.5	1	75
mesoporous silica	PEI	4.5	1	75
poly(methyl methacrylate)	PEI	4.4	1	50
Mil-101Cr	-NH_2 groups	4.3	1	20
silica microspheres	TEPA	4.3	1	75
silica microspheres	TEPA	2.6	1	35
mesoporous silica	PEI	2.6	1	30
silica aerogel	amino-alkyl-trialkoxysilane	2.4	0.81	40
nanoclay	APTMS	1.8	1	85
pore expanded silica	APTES	1.2	1	30
TiO_2/ZrO_2	APTMS	0.58	1	30
macroporous silica	linear poly-L-alanine	3.9	0.1	50
mesoporous silica	TEPA	3.5	0.1	75
fly ash extraction	PEI	3.3	0.1	90
silica gel	PEI+PZ	3.2	0.1	75
MCM-41 modified by carbon black	(3-trimethoxysilylpropyl) diethylenetriamine	1.7	0.05	25
mesoporous silica	(3-trimethoxysilylpropyl) diethylenetriamine	1.6	0.15	60
nanoclay	APTMS	1.6	0.1	85
Mil-101Cr (MOF)	-NH_2 groups	1.6	0.15	20
polymer/silica hollow fibers	APTMS	1.0	0.1	35
polymer/silica hollow fibers	PEI	1.0	0.14	35
TiO_2/ZrO_2	APTMS	0.41	0.1	30

Modification of sorbents using amines can be split into three distinct classes: 1) physical impregnation of an amine functional groups amines into an adsorbent, 2) post-chemical grafting of amines to the adsorbent, and 3) in-situ chemical grafting of an amine group to the adsorbent (Dutcher, Fan, and Russell 2015). It has been reported by Dutcher et al. (2015) that using the physical impregnation method (Class 1) usually produces an MOF with higher CO_2 adsorption capacity than the other classes of modification methods. Polyethyleneimine (PEI) and tetraethylenepentamine (TEPA) are the most commonly used compounds for modifying the sorbents due to being less volatile and being polyamines, or amine polymers. Amine polymers usually have a large number of amino groups, which translates to higher CO_2 adsorption capacity (Dutcher, Fan, and Russell 2015).

Class 2 and 3 of amine modification methods are not viable for ZIF-8 due to its small pore size (Ding et al. 2018). However, Xian et al. (2015) have investigated class one

modification (i.e., physical impregnation) of ZIF-8. They were able to successfully incorporate linear PEI into a ZIF-8 produced in DMF using a solvothermal synthesis method. Compared to the unmodified ZIF-8, impregnation of ZIF-8 with PEI exhibited higher CO_2 adsorption capacity (1.2 mmol/g) and a selectivity (relative concentration of CO_2 to N_2) of 25.4 with increased PEI loading (Xian et al. 2015). These enhancements in CO_2 sorption capacity occurred even though surface area and pore volumes of the ZIF-8 decreased significantly as a result of the modifications. Furthermore, the modified ZIF-8 in the study by Xian et al. (2015) exhibited high CO_2 adsorption capacity (0.9-1.1 mmol/g) at very low pressures (0 - 0.15 bar), the CO_2 sorption capacity also increased with higher water vapor concentrations, and higher adsorption took places at higher temperatures (338 K). These qualities are rare amongst MOFs. Therefore, the current thesis aimed at improving and optimizing the ZIF-8 produced by Xian et al. (2015) through a) synthesis of the ZIF-8 using more eco-friendly solvents and b) replacing the linear PEI used in their study by branched PEI in an effort to increase the CO_2 adsorption capacity above the levels achieved by Xian et al. (2015).

3. MATERIALS AND METHODS

3.1 Materials

Zinc nitrate hexahydrate [$Zn(NO_3)_2.6H_2O$] and methanol [MeOH] were obtained from Fisher Scientific, 2-methylimidazole (HMIM) was obtained from Acros Organics, and branched polyethyleneimine (MW 1200) was obtained from PolySciences, Inc. All chemicals were used without further purification. Industrial grade carbon dioxide and nitrogen gas cylinders were obtained from Praxair.

3.2 Synthesis of ZIF-8

Synthesis of ZIF-8 was performed using two different solvents, methanol and DI water to produce ZIF-8-MeOH and ZIF-8-DI, respectively. These solvents were chosen because they are more environmentally preferable compared to Dimethylformamide (DMF). According to (Joshi and Adhikari 2019), DMF can cause abdominal pain, nausea, vomiting, liver damage, and other adverse health effects. DMF can enter the body dermally and so methanol and water are better solvents to use for synthesis.

The ZIF-8 was synthesized based on the reaction illustrated in Figure 14. The zinc, provided by the zinc-nitrate salt, is bonded with the nitrogen atoms of the imidazolate anions, which are provided by the 2-methylimidazole molecules. This reaction produces a three-dimensional sodalite (sod) structure of ZIF-8 that has a large pore volume (Figure 15). The sodalite structure is one of the many topologies that zeolites can take.

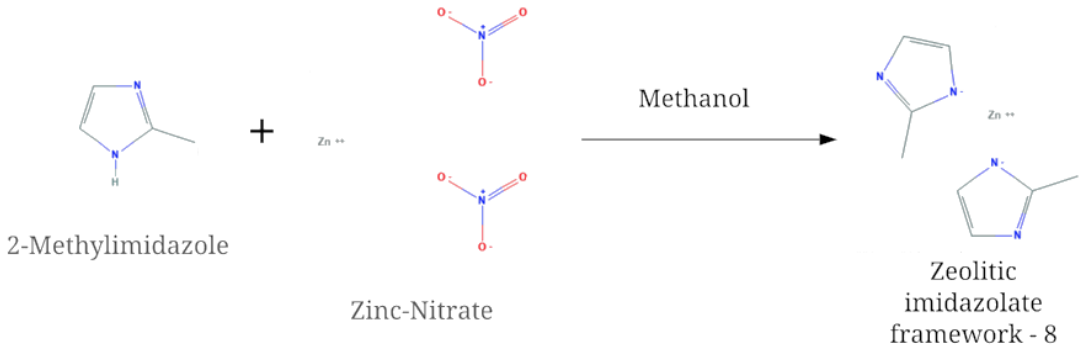

Figure 14. Preparation of ZIF-8 with HMIM and hydrated zinc salt. Reproduced from Chemical Structures, National Center for Biotechnology Information. PubChem Database

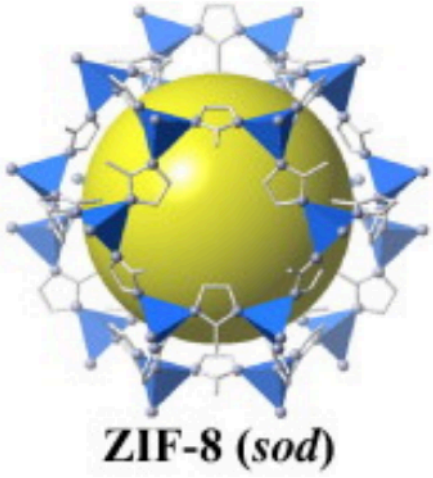

Figure 15. A sodalite (sod) cage of ZIF-8, pore volume, metal cluster, and organic linker shown in yellow, blue, and white, respectively (Reproduced from Lee et al. 2015)

ZIF-8 was synthesized according to a solvothermal method reported by Ta et. al (2018) with slight modifications in the drying method to produce a higher ZIF-8 yield. The drying method used by Ta et. al (2018) was vacuum drying at 120°C, while this study used oven drying at 100°C. To produce ZIF-8, zinc nitrate hexahydrate was dissolved in half

of the desired volume of methanol and labeled solution A. 2-Methylimidazole was dissolved in the remaining volume of methanol and labeled solution B. Solution A was mixed with Solution B to create the final mixture with a composition of 1:4:20 (mol Zn: mol HMIM: mL MeOH). This mixture was left for 6 hours to react at 50 °C without stirring. The mixture turned from a clear solution to a milky white suspension as shown in Figure 16a. This suspension was then centrifuged at 5000 rpm for 10 minutes, washed three times with methanol, and dried in an oven at 100°C to produce the ZIF-8 white powder shown in Figure 16b. The product ZIF-8 was kept in a desiccator until further characterization and use.

a)

b)

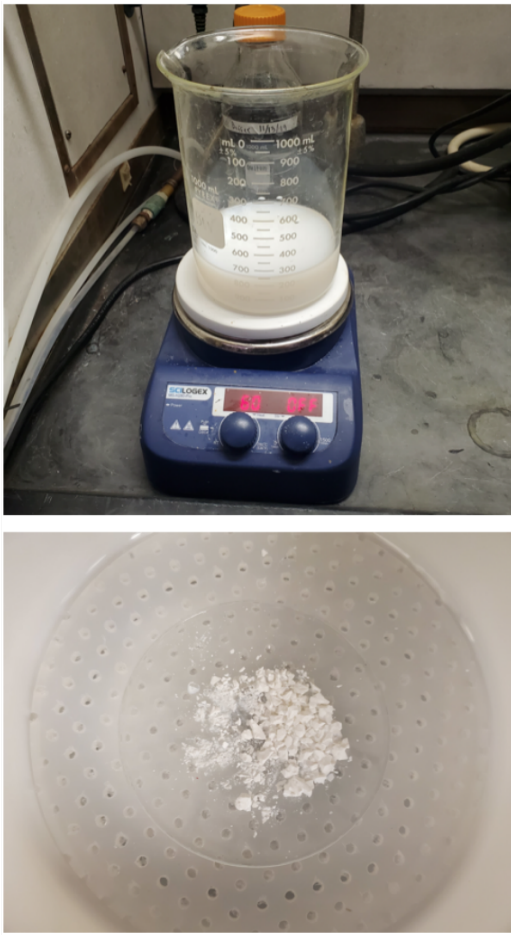

Figure 16. ZIF-8 prepared in methanol a) ZIF-8 solution before drying and centrifugation and b) dry ZIF-8 product

Another method that uses DI water as the solvent instead of methanol for making ZIF-8 was also investigated. This ZIF-8 was synthesized according to the method reported by Jian et.al (2015) with modifications. The difference between the method used in this thesis and the original one developed by Jian et al. (2015) were the use of different metal salt precursors as well as different molar ratios of the reactants. The purpose of these modifications was to increase the crystallinity of ZIF-8 and improve other characteristics.

To produce ZIF-8 in water, Zinc nitrate hexahydrate was dissolved in half of the desired amount of water and labeled solution A. 2-Methylimidazole was dissolved in the remaining water volume and labeled solution B. Solution A was mixed with Solution B to create a mixture with a composition of 1:70:310 (mol Zn: mol Hmim: mol DI water). This mixture was left to react for 16 hours at room temperature without stirring. The resulting suspension was centrifuged at 7000 rpm for 5 minutes, washed three times with DI water, and then dried in an oven at 60 °C to produce a white powder similar to that shown in Figure 3-3b. Yields were not reported due to the loss of ZIF-8 when transferring from container to container.

3.3 Modification of ZIF-8 with bPEI

The main reason for modifying ZIF-8 with bPEI in this study was not only to increase its sorption capacity but also to improve selectivity for CO_2 when there are multiple gases that compete for the sorption sites. However, the selectivity evaluation was not performed in the current study because the modification with bPEI negatively affected the sorption capacity of ZIF-8-MeOH.

ZIF-8 was modified using branched polyethyleneimine (bPEI) according to a wet impregnation method reported by Xian et. al (2015) with modifications in the solvent

used, activation method, and sonication technique. Xian et. al (2015) reported vacuum activation for 12 hours at 423 K, while this study performed the activation at 423 K overnight in a conventional oven. Xian et. al (2015) also reported using 2 mL of methanol which was an insufficient amount for sonication, so this study used 5 mL of methanol. In this study, the bPEI solution was mixed with ZIF-8 then sonicated, while Xian et.al (2015) added the solution drop by drop. The mechanisms of impregnation of the ZIF-8 with bPEI is illustrated in Figure 17. The actual process used for impregnation of ZIF-8 is described below.

A mass of 0.0450 g of bPEI was dissolved and sonicated in 5 mL of methanol. Next, the bPEI solution was added to 0.1 g of dry ZIF-8 and the resulting suspension was sonicated for 5 minutes. Subsequently, the suspension was placed in an oven at 75 °C for 3 hours and then was left in a desiccator to dry overnight. The dry product, named hereafter ZIF-8-MeOH-45bPEI, is shown in Figure 18. It is a white powder similar in appearance to the unmodified ZIF-8, but has a slight adhesive quality reminiscent of the bPEI.

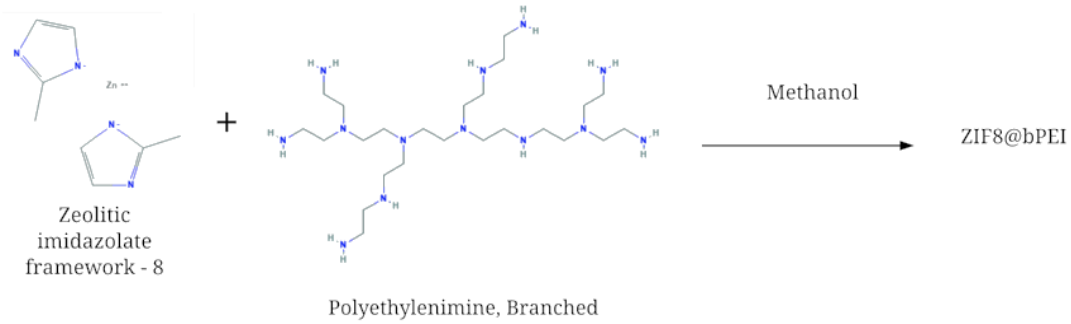

Figure 17. Modification of ZIF-8 with bPEI. Reproduced from Chemical structures from National Center for Biotechnology Information. PubChem Database

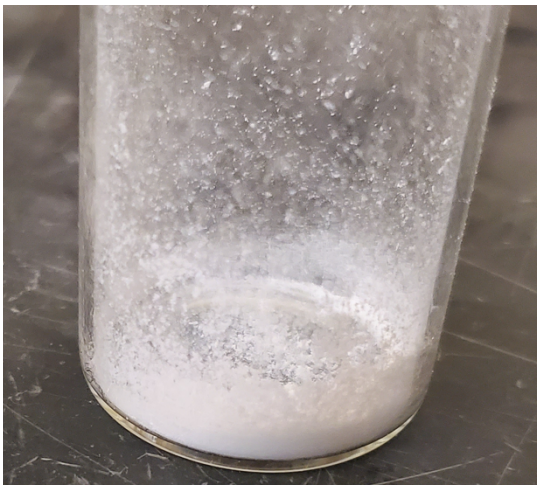

Figure 18. ZIF-8 modified with bPEI

3.4 Characterization of ZIF-8

Both the unmodified and bPEI-modified ZIF-8 powders were characterized using x-ray diffraction spectroscopy (XRD) to determine the crystal structure, Fourier transform infrared spectroscopy (FTIR) to examine chemical properties, thermal gravimetric analysis (TGA) to observe decomposition temperatures and determine bPEI loading, and Brunauer-Emmett-Teller (BET) analysis to determine the surface area of the ZIF-8.

The XRD instrument used was a Siemens D5000 Diffraktometer and was operated under the following conditions: flow rate greater than 4 L/min, voltage of 40 kV, current of 30 mA and a scan speed of 5 °/min. The range analyzed was 0 to 35° on a 2θ scale. The FTIR used was a Jasco FT/IR-4600 with ATR diamond. The samples were analyzed in the range of 400 cm^{-1} to 4000 cm^{-1}. The TGA model used was a Mettler Toledo TGA/SDTA851e. All TGA samples were tested under nitrogen gas flow and heated at a rate of 15 °C/min. The unmodified ZIF-8 was analyzed in the temperature range of 0 to 600°C while the ZIF-8 modified with bPEI was analyzed in the range of 0 to 330 °C. The bPEI-modified ZIF-8 was tested at a lower temperature due to issues encountered with

the TGA at the time of testing. However, bPEI has a decomposition temperature that is lower than 330°C (Xian, et.al 2015) and therefore operating the TGA at this temperature range should have been sufficient for detecting decomposition of bPEI. Decomposition temperatures were determined to be when weight loss equated to 10% in one drop. The BET analyzer model was the Quantachrome Instruments, Monosorb Rapid Surface Area Analyzer and was operated under the conditions of 6 psi and 21 psi of nitrogen and air, respectively and at a current of 230 mA.

3.5 Design and Description of the CO_2 Adsorption Apparatus

A custom-made gravimetric system using a quartz crystal microbalance (QCM) was used to quantify the CO_2 sorption capacity of ZIF-8 under a range of pressures (≤ 1 bar) that are representative of flue gases from post-combustion processes.

3.5.1 QCM Theory and Considerations

The quartz crystal operates under the piezoelectric effect, where the quartz crystal returns an electric charge when a mechanical stress is applied to it. When an alternating current is applied to the quartz crystal, it oscillates at a resonance frequency f_0. Any change to the resonance frequency (Δf_0) can be attributed to the following factors: a mass deposited (f_m) on the crystal surface; a change in temperature (f_T), pressure (f_p), slippage (f_{sl}), density and viscosity of the media around the crystal (f_η); and/or the change in surface roughness (f_R) of the crystal (Wu et al. 2004). The resulting equation to quantify the change in resonance frequency is shown below.

$$\Delta f_0 = \Delta f_m + \Delta f_p + \Delta f_T + \Delta f_{sl} + \Delta f_\eta + \Delta f_R \quad (4.1)$$

Equation 4.1 can be simplified according to the design configurations of the system used in the current study. Since the temperature of the experiments were constant at 25 °C, Δf_T can be removed from the equation because the quartz crystals provided by Inficion Inc. experience a negligible frequency change in the temperature range of 20°C to

100°C. The frequency change due to slippage and viscosity of the media, $\Delta f_{sl} + \Delta f_{\eta}$, can be disregarded from the equation because the medium is a gas not a liquid (Kashan et al. 2017). The last term that can be neglected is the surface roughness of the crystal, Δf_R, because the crystals provided by Inficon Inc. are polished and studies have shown that polished crystals cause minimal frequency changes as a result of alterations in surface roughness (Wu et al. 2004). Therefore, Equation 4.1 simplifies to Equation 4.2.

$$\Delta f_0 = \Delta f_m + \Delta f_p \tag{4.2}$$

The change in frequency of the crystal caused by foreign deposits Δf_m can be determined using Equation 4.3, which is known as the Saurbrey equation. Δf_m is dependent on the resonance frequency (f_0 = 6 MHz), the change in mass of the crystal (Δm), the density ($\rho_q = 2.649$ g/cm^3), the shear modulus ($\mu_q = 3.32 \times 10^{11}$ dynes/cm^2) of the crystal, and the area of the crystal (A = 1.53 cm^2). Equation 4.3 only holds if the frequency shift caused by the mass deposited is less than 2% of the resonance frequency (Alassi, Benammar, and Brett 2017).

$$\Delta f_m = -\frac{2f_0^2}{\sqrt{\mu_q \rho_q}} \frac{\Delta m}{A} \tag{4.3}$$

The change in frequency caused by pressure (Δf_p) can be calculated using Equation 4.4 and is dependent on the fundamental frequency of the quartz crystal (f_0) and the pressure of atmosphere (Tsionsky et al. 1995).

$$\Delta f_p = [(1.06 * 10^{-6}) f_0] P \tag{4.4}$$

The following sequential steps were used to calculate the mass of CO_2 adsorbed onto the ZIF-8 samples:

1. The frequency values at each pressure point were recorded for the reference crystals. The frequency value at maximum vacuum (0.08 bar) was measured and deemed the resonant frequency (f_0).
2. The frequency values from step 1 were subtracted from the resonant frequency, f_0, to obtain Δf_p at each pressure point. This was an alternative approach to using Equation 4.4 to determine Δf_p.
3. The crystals loaded with ZIF-8 samples were tested at each pressure point and the frequency values were recorded.
4. The frequency value at maximum vacuum for the crystals loaded with ZIF-8 samples were subtracted by the resonant frequency (f_0) to determine from just the mass of ZIF-8 only ($\Delta f_{m\_deposited}$).
5. The frequency values obtained in step 3 were then subtracted by the Δf_p obtained in step 2, to determine Δf_m at each pressure point. This Δf_m includes the mass deposited by the ZIF-8 samples ($\Delta f_{m\_deposited}$) and mass of CO_2 adsorbed ($\Delta f_{m\_adsorbed}$).
6. $\Delta f_{m\_deposited}$ from step 4 is subtracted from Δf_m in step 5 to obtain the mass of CO_2 adsorbed ($\Delta f_{m\_adsorbed}$).

3.5.2 Description of the QCM Apparatus

3.5.2.1 Quartz Crystal Microbalance (QCM) Components

The quartz crystal microbalance, oscillator, and quartz crystals utilized for the CO_2 measurement setup were a single front load sensor (Figure 19), STM-2 or oscillator, and 6 MHz gold crystals, respectively, all manufactured by INFICON Inc. A typical setup of the quartz crystal microbalance is shown in Figure 20. The front load single sensor loaded with the quartz crystals is connected to the STM-2 oscillator that is linked to the

STM-2 Software Interface to monitor the frequency changes of the quartz crystal (Figure 21).

Figure 19. Front load single sensor (Reproduced from Inficon Inc.)

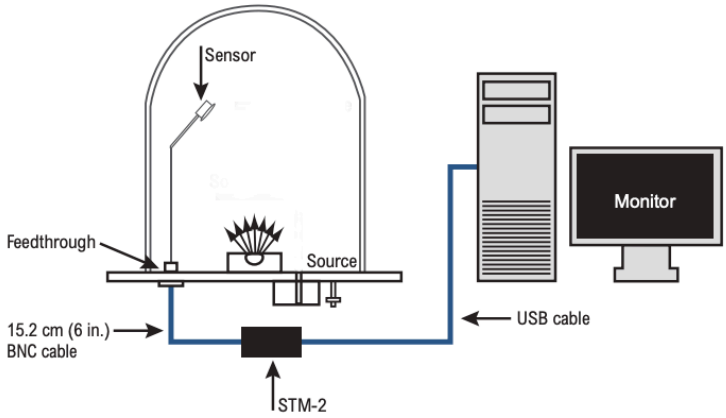

Figure 20. Common setup of a QCM system (Reproduced from Inficon Inc.)

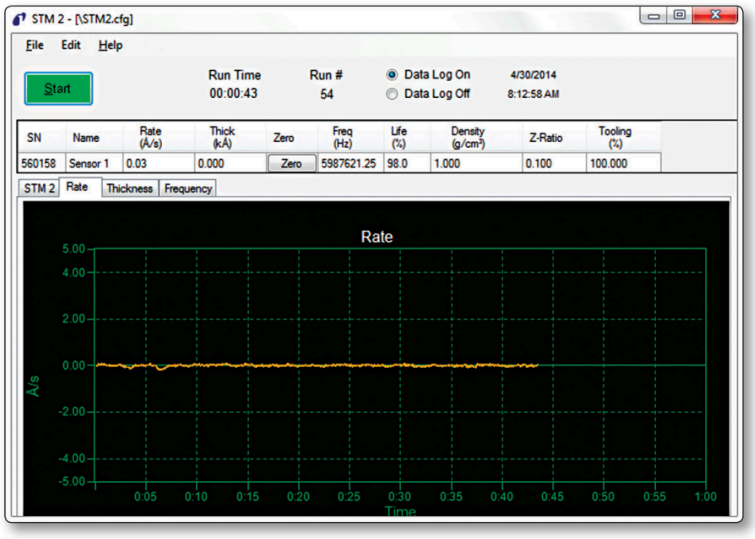

Figure 21. STM-2 Software Interface (Reproduced from Inficon Inc.)

3.5.2.2 Vacuum Chamber

With the aforementioned testing requirements for flue gas pressure, a stainless steel vacuum chamber was designed to house the QCM sensor head. The drawings of the designed vacuum chamber were sent to Nor-Cal Products, Inc. for manufacturing the chamber. A schematic of the vacuum chamber is presented in Figure 3-9. The chamber was sized to be 10 inches in diameter and 4 inches in height with a port for the quartz crystal microbalance and 2 ports for the gas inlet and outlet. The diameter was constrained by the length of the quartz crystal microbalance, which was 8 inches in length and the height was constrained by the thermometer stem.

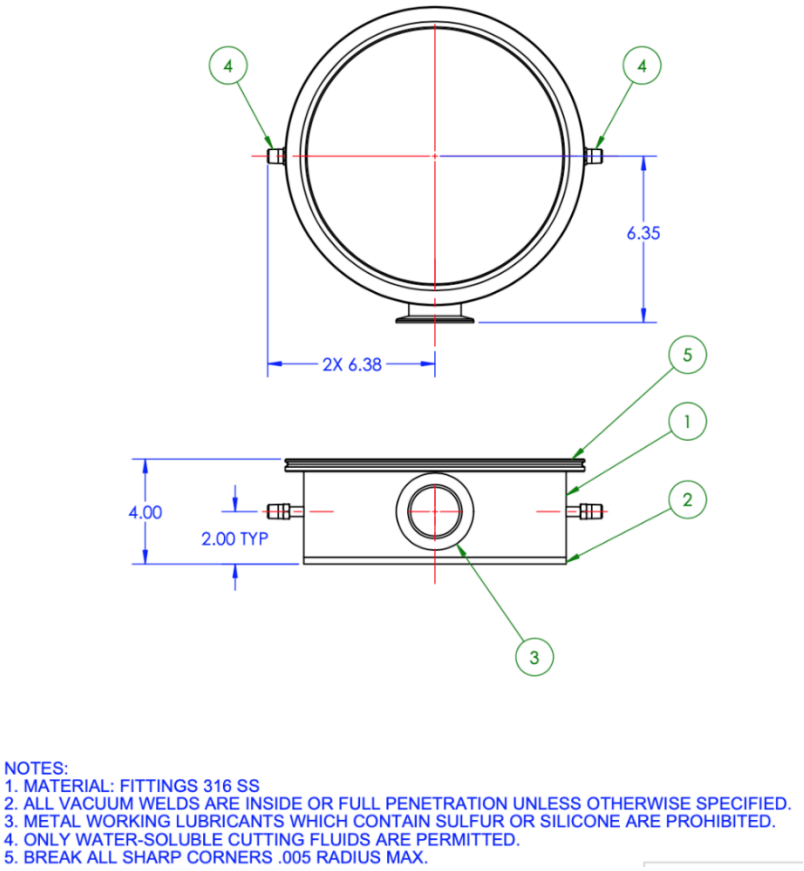

Figure 22. Vacuum chamber design (Nor-cal Products Inc.)

3.5.3 Description of the CO_2 Sorption Testing Assembly

The previously described vacuum chamber and the quartz crystal microbalance components constitute the main elements of the CO_2 sorption testing assembly illustrated in Figure 23. This assembly was adapted from CO_2 sorption testing systems used in the literature (Hesketh, Nair, and Sulchek n.d.). The QCM was placed in the vacuum chamber and BNC connectors were connected to the STM-2 Rate/Deposition Monitor. The STM-2 was connected to a laptop where the STM-2 software was used to monitor the frequency change of the quartz crystal during the experiment. The temperature in the vacuum chamber was monitored with a temperature gauge placed on

top of the chamber. The pressure in the chamber was monitored using a vacuum pressure gauge. Stainless steel pipe fittings purchased from McMaster Carr were used to connect the system together. The vacuum gauge was used in conjunction with a needle valve placed on the gas exit side to maintain a consistent pressure in the chamber. A vacuum pump, purchased from McMaster Carr, was utilized to apply the required vacuum pressure inside the test chamber. The gas inlet side was equipped with needle valves and pressure regulators to control the flow of the CO_2 and nitrogen gases to the vacuum chamber.

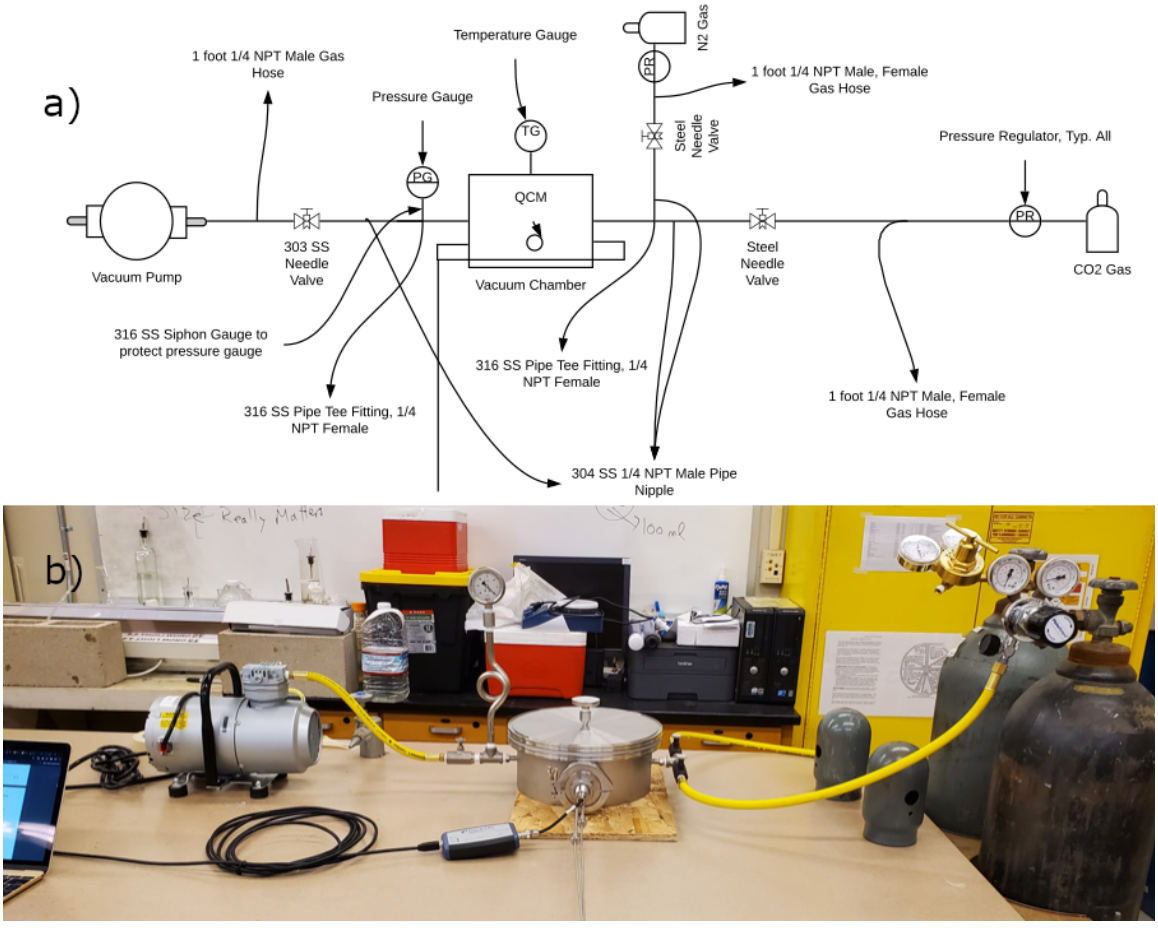

Figure 23. The CO_2 adsorption testing apparatus a) schematic b) picture of the actual system

3.5.4 Sample Deposition

Considering the quartz crystals have an electrode coating on the bottom as shown in Figure 24a, the modified and unmodified ZIF-8 samples were deposited on the top of the quartz crystal, shown in Figure 24b, using a drop casting technique. The ZIF-8 was first sonicated using a probe sonicator in 5 mL of methanol for 2 minutes and then 10 µl of this suspension was pipetted and deposited onto the quartz crystals. The quartz crystals were then dried in a desiccator for 20 minutes. Once dry, the crystals were wiped with Kimwipes^{TM} prior to testing to remove the sample materials that did not adhere to it to ensure that the crystal would properly oscillate.

Figure 24. Quartz crystals used in the study a) the bottom side has the electrodes that are in contact with the crystal holder b) the top side where the sample is deposited and is in contact with the CO_2 gas

3.5.5 Testing Procedure

Blank quartz crystals were first removed from the crystal storage container using a Teflon tweezer, cleaned with isopropyl alcohol, and then dried for 3 minutes in an oven at 75°C. One quartz crystal was placed in the crystal holder of the QCM before closing the vacuum chamber. The vacuum chamber was then exposed to the lowest vacuum that the vacuum pump could achieve, which was 0.08 bar (27.5 in Hg) vacuum pressure.

Once the frequency stabilized, it was recorded, then the vacuum pump was throttled using a needle valve and the desired gas was slowly let into the system to reach the next pressure point. Each blank quartz crystal was tested in triplicate. After each blank quartz crystal was tested, it was coated by the drop casting technique mentioned previously. In total triplicate quartz crystals loaded with ZIF-8 samples were tested at each pressure point. The blank as well as the loaded crystals were tested on the same day to minimize errors that can result from variations in the surrounding environmental conditions (e.g., temperature and humidity).

4. RESULTS AND DISCUSSION

4.1 Unmodified ZIF-8

The characteristics of the synthesized MOFs (ZIF-8-MeOH and ZIF-8-DI) were determined using FTIR, XRD, TGA, and BET analyses and the results are presented in section 4.1.1. ZIF-8-MeOH was also tested for CO_2 & N_2 adsorption and the results are presented in section 4.1.2.

4.1.1 Characteristics of the Manufactured MOFs

The FTIR spectrum of synthesized ZIF-8-MeOH shown in Figure 25 is in good agreement with the literature (Ta et al. 2018). This is shown by the peaks at 1585 cm^{-1}, 1458 cm^{-1}, 1425 cm^{-1},1307 cm^{-1}, 1175 cm^{-1}, 1145 cm^{-1}, 1092 cm^{-1}, 994 cm^{-1}, 953 cm^{-1}, 752 cm^{-1}, 693 cm^{-1}, and 421 cm^{-1}. Specifically, the lack of a peak at 1850 cm^{-1} and the presence of a peak at 1145 cm^{-1} indicate conversion of imidazole into imidazolate (Figure 4-1b). Imidazole comes from the organic linker, Hmim used in the synthesis of ZIF-8, and is deprotonated when it reacts with the solvent. The band at 421 cm^{-1} shows that there is a Zn-N bond (Figure 4-1c). The band at 1585 cm^{-1} corresponds to a C=N double bond (Figure 4-1a) while the bands found from 1350 cm^{-1} to 1500 cm^{-1} correspond to a cyclic bond. The band at 758 cm^{-1} corresponds to vibrations outside the cyclic bond. This confirms that the product of the synthesis process was ZIF-8 as evidenced by the appearance of the metal ion Zn and the functional group imidazolate.

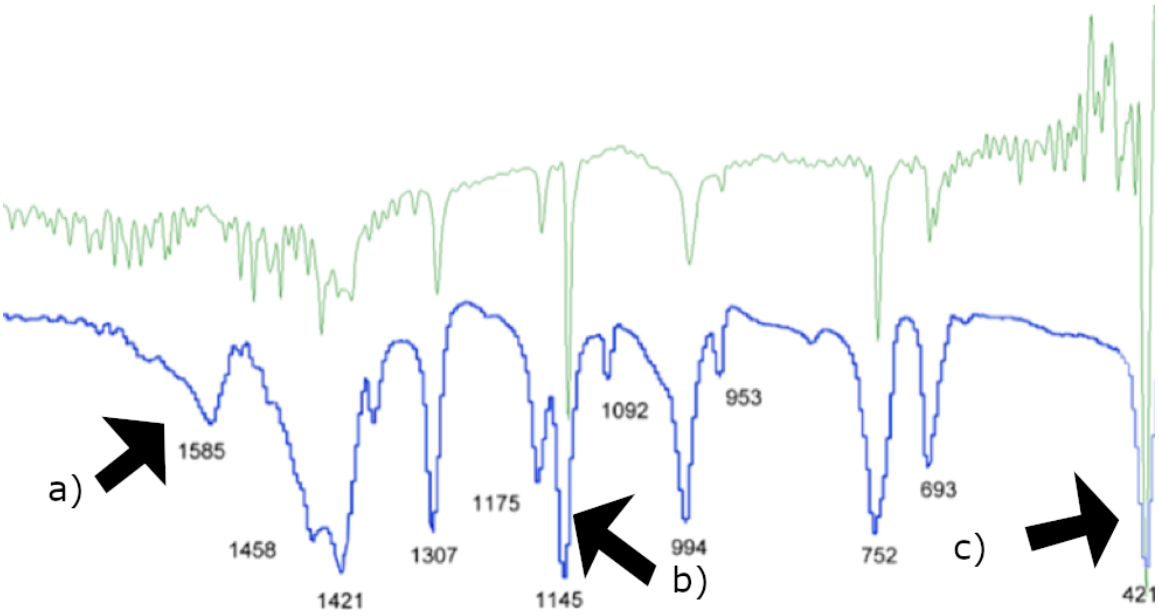

Figure 25. FTIR spectra of ZIF-8-MeOH (green) and ZIF-8 produced by Ta et.al 2018 (blue)

The ZIF-8-DI was also confirmed to match the FTIR spectra of ZIF-8-MeOH as well as ZIF-8 made in water by Jain et al. (2015) as shown in

Figure 26. ZIF-8-DI had the characteristic peak of the Zn-N bond at 418.7 cm^{-1} (Figure 4-2b), imidazolate at 1141.9 cm^{-1} (Figure 4-2c), and C=N double bond at 1581.2 cm^{-1} (Figure 4-2a). Although most peaks were similar to what was reported by Jian et al. (2015), there were undetermined peaks (Figure 4-2) that could be a result of differences in the synthesis processes as outlined in Section 3.2. Changes in amount of solvent used, choice of metal salt precursor, and reaction time may have caused the aforementioned unknown peaks to appear. Furthermore, the FTIR spectrum of the ZIF-8 produced using methanol and water was overall similar to that of ZIF-8-DMF as seen in Figure 27 (Xian et. al 2015).

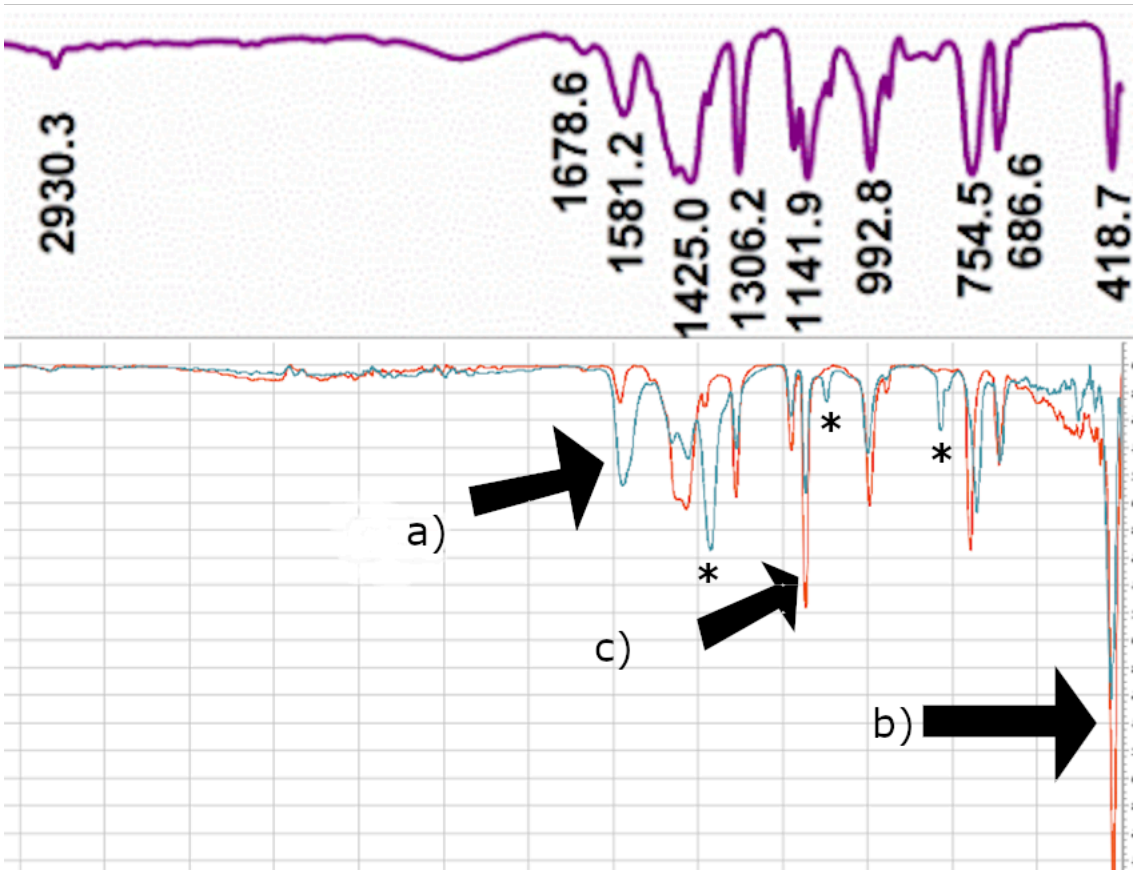

Figure 26. ZIF-8-DI (blue), ZIF-8-MeOH (red) and ZIF-8-DI produced by Jian et al. (2015) (purple)

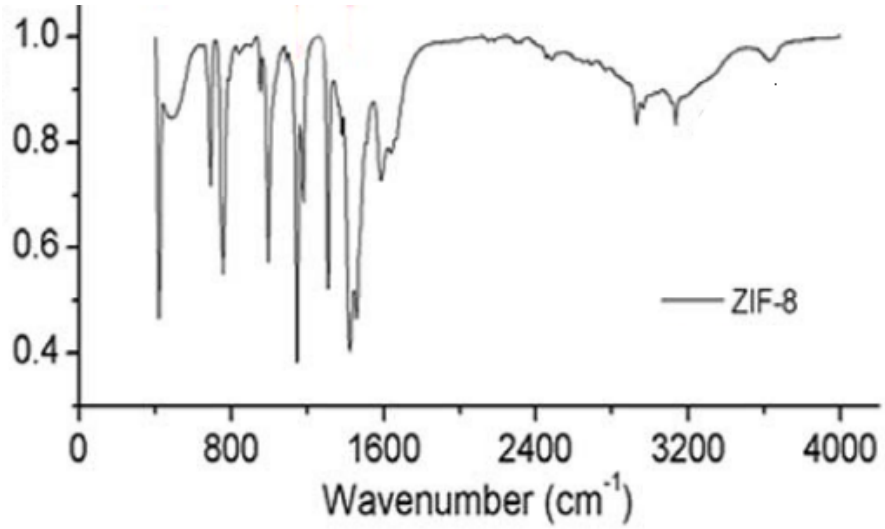

Figure 27. FTIR Spectra of ZIF-8 prepared with DMF (Reproduced from (Zhang et al. 2013)*)*

The BET surface area analysis showed that ZIF-8-MeOH had a surface area of 1300 m^2/g. This is slightly lower than the surface area of ZIF-8-MeOH produced by Ta et al. (2018), which was 1576 m^2/g. One potential reason for this difference in surface area may have been the use of oven drying instead of vacuum oven drying, which was the one factor that differed from the synthesis protocol by Ta et al. (2018). ZIF-8-DMF reported by Xian et. al (2015), had a surface area of 1150 m^2/g, which is lower than the ZIF-8-MeOH synthesized in this study. Overall, these data show that the ZIF-8-MeOH produced in this study had a surface area comparable to other types of ZIF-8 made in less eco-friendly solvents.

The water based ZIF-8 synthesized in this study had a surface area of 732 m^2/g, which is drastically lower than the ZIF-8-MeOH. Additionally, this surface area is much lower than the surface area of the water-based ZIF-8 produced by Jian et al. (2015), which was 1132 m^2/g. It is noted that the ZIF-8-DI was synthesized following the method by Jian et al. (2015) but with some modifications that included the use of a different metal precursor (zinc nitrate hexahydrate instead of zinc acetate dehydrate) and a lower water volume. Therefore, the observed difference in surface area is likely attributed to such modifications. Considering the water based synthesis produced a ZIF-8 with a low surface area, this method was not pursued further for CO_2 sorption testing or modification purposes, based on the assumption that surface area correlates with CO_2 adsorption capacity.

The XRD of the methanol based ZIF-8 sample is presented in Figure 28. The peaks shown in Figure 28 are in good agreement with XRD data found in literature (Ta et al. 2018).This confirms the successful manufacturing of ZIF-8. Furthermore, the main peaks and their Miller indices calculated using the XRD data matched those of the ZIF-8-MeOH synthesized by Ta et al. (2018) as shown in Figure 28. The calculations are validated by

the lattice constants (a_0) which are consistent amongst all the peaks and ZIF-8 was determined to be a cubic structure.

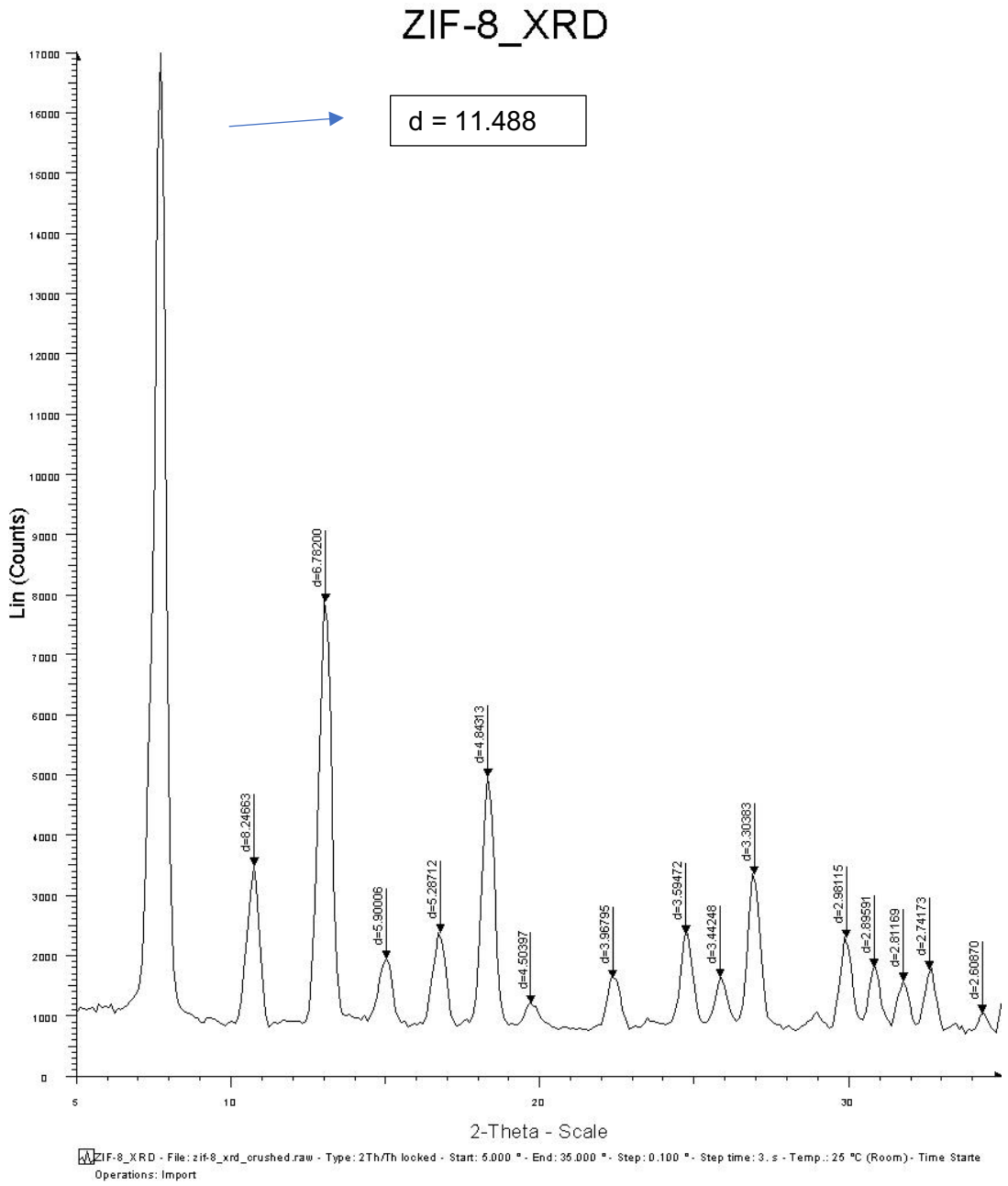

Figure 28. XRD of ZIF-8-MeOH

Table 5. Mathematical Determination of d-spacing of ZIF-8 MeOH

Peak No.	2θ (°)	$\sin^2\theta$	$1*(\sin^2\theta/\sin^2\theta_{min})$	$2*(\sin^2\theta/\sin^2\theta_{min})$	$3*(\sin^2\theta/\sin^2\theta_{min})$	h2+k2+l2	hkl	a_0	d-spacing (Å)
1	7.7	0.0045	1	2	3	2	011	16.2	11.488
2	10.8	0.0089	1.978	3.956	5.933	4	002	16.5	8.247
3	13.0	0.0128	2.844	5.689	8.532	6	112	16.6	6.782
4	15.0	0.0170	3.778	7.556	11.333	8	022	16.7	5.900
5	16.8	0.0213	4.733	9.467	14.200	10	013	16.7	5.287
6	18.5	0.0258	5.733	11.467	17.200	12	222	16.8	4.843

The ZIF-8-DMF synthesized by Xian et. al (2015) exhibited a similar crystal structure to that of ZIF-8-MeOH as shown in Figure 29. This conclusion was deduced because the XRD peaks are found at the same theta location, indicating similar d-spacings and similar miller indices to the ones observed herein. These XRD data indicate that ZIF-8-MeOH have high crystallinity like ZIF-8-DMF. This indicates that creating ZIF-8 with methanol can produce just as high of crystallinity as DMF.

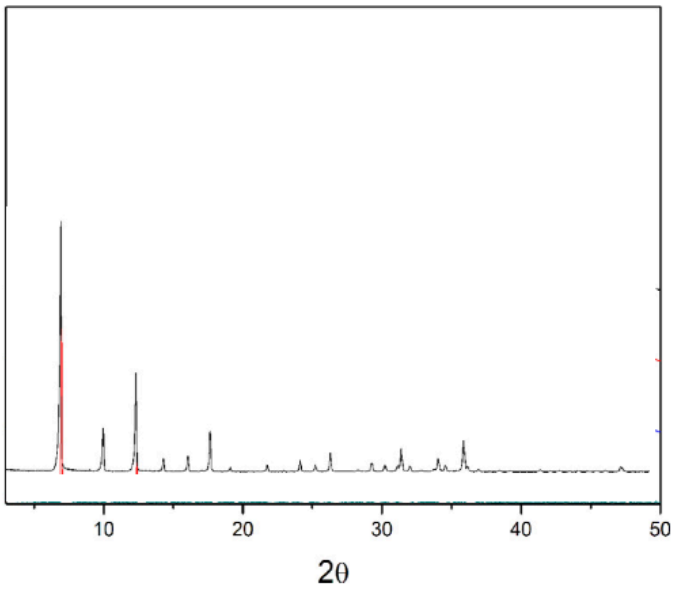

Figure 29. XRD of ZIF-8 made with DMF (reproduced from (Xian et al. 2015)

The TGA profile of ZIF-8-MeOH is presented in Figure 30. This TGA data indicate that ZIF-8-MeOH had a decomposition temperature of ~ 460 °C, which is close to the decomposition temperature of 475 °C reported by Ta el al. (2018) for their ZIF-8-MeOH. The ZIF-8-DMF reported by Xian et al. (2015) also had a similar decomposition temperature of ~775 K (~500°C) as shown in Figure 31.

Overall, the TGA profile shown in Figure 30 is in agreement with that reported by Ta el al. (2018) except for the slight difference in the decomposition temperature. Furthermore, the TGA results show the high thermal stability of ZIF-8-MeOH as indicated by the relatively steady downward slope of the weight loss that begun at around ~ 450 °C. This makes ZIF-8 suitable for withstanding temperatures of flue gases from post-combustion carbon that reach 150°C (Samanta et al. 2012). It is noted that the slight increase of weight at the beginning of the TGA analysis profile in Figure 30 was likely due to the adsorption of N_2 gas by the sample.

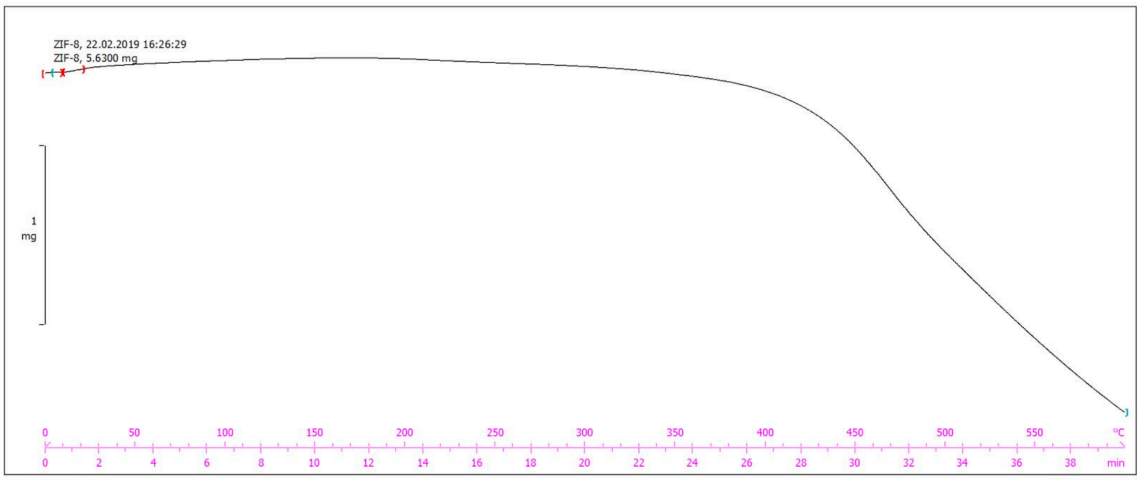

Figure 30. Experimental TGA results for ZIF-8-MeOH made in this study heated from 0-600°C. Y-axis is weight (mg).

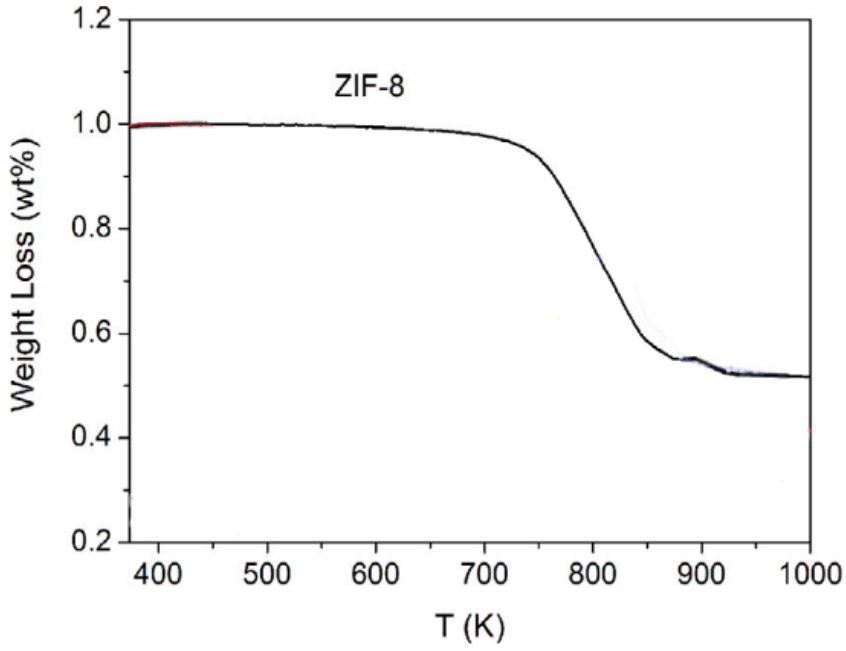

Figure 31. The TGA result of ZIF-8-DMF (reproduced from Xian et. al 2015)

Overall, the characterization data presented herein for ZIF-8-MeOH and the literature data for ZIF-8-DMF show that both ZIF powders were comparable in structure and composition, but slightly differed in surface area.

4.1.2 CO_2 &N_2 Adsorption Capacity of ZIF-8

The CO_2 sorption capacity of the ZIF-8-MeOH was studied in the relative pressure range of 0.3 – 1.0 (p/p^0). The relative pressure (p/p^0) is the ratio of the tested pressure (p) to the atmospheric pressure (p^0). The 0.3 -1.0 p/p^0 range was chosen as it is representative of flue gas conditions (Wang et al. 2017). Lower relative pressures (0.15) are also worthy of testing because flue gases can reach those low levels but they could not be achieved due to equipment limitations.

The equilibrium amount of CO_2 sorbed on ZIF-8-MeOH increased linearly with the increase in CO_2 relative pressure as shown in Figure 32. This proves the hypothesis that the methanol based ZIF-8 can serve as an effective solid sorbent for CO_2. Furthermore, the sorption capacity of this ZIF-8-MeOH is comparable to that of the less eco-friendly DMF-based ZIF-8 as seen in Figure 32. At atmospheric pressure, for example, the ZIF-8-MeOH adsorbed 0.85 mmol/g, which is slightly higher than the 0.75 mmol/g achieved by ZIF-8-DMF. This CO_2 sorption data correlates with the surface area results presented earlier. The ZIF-8-MeOH has a surface area of 1300 m^2/g compared to 1150 m^2/g for ZIF-8-DMF.

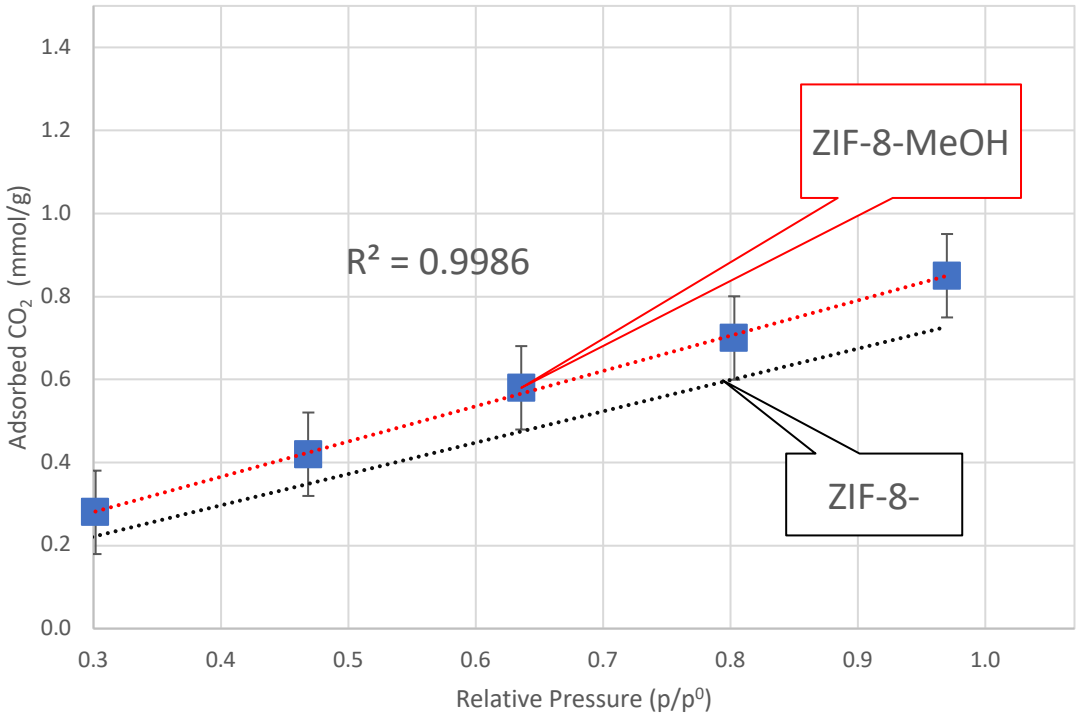

Figure 32. CO_2 adsorption results for ZIF-8-MeOH and ZIF-8-DMF (ZIF-8-DMF data reproduced from Xian et. al 2015)

It is noted that the CO_2 adsorption experiments by Xian et al. (2015) were performed using a surface area and porosity system, micromeritics ASAP 2020, while the experiments in this study were conducted using a quartz crystal microbalance setup. The micromeritics ASAP 2020 conducts physisorption and chemisorption studies using BET theory. A study by (Sarango et al. 2018) compared CO_2 adsorption capacity of ZIF-8 at atmospheric pressure and 25°C using the BET method and QCM. The study found that 0.73 mmol/g of CO_2 was adsorbed by ZIF-8 through the BET method while 0.63 mmol/g was adsorbed using the QCM. This implies that the QCM is of sufficient accuracy to detect CO_2 adsorption and that the QCM assembly used herein was working as intended.

ZIF-MeOH was also tested with N_2 to check if it had a higher affinity for CO_2. This is important because flue gases usually have high amounts of N_2 and lower amounts of CO_2 (Wang et al. 2017). Both the ZIF-8-MeOH synthesized herein and the ZIF-8-DMF synthesized by Xian, et al. (2015) adsorbed 0.15 mmol/g of N_2 at atmospheric pressure. These results indicate that ZIF-8 has an affinity to sorb N_2 but it is much lower than its affinity to sorb CO_2. It is noted that despite the similarity of N_2 adsorption results obtained herein to those reported in the literature values, tests run on ZIF-8 modified with bPEI indicated there was a sensitivity issue with the QCM system. Therefore, the N_2 adsorption results obtained were deemed inconclusive and the QCM system needs to be modified to ensure that the N2 adsorption data are accurate.

4.2 Modified ZIF-8

To improve the adsorption capacity and selectivity for CO_2, the ZIF-8-MeOH was modified with branched PEI (bPEI). The characterization results are presented in Section 4.2.1 while the CO_2 adsorption capacity results are presented in section 4.2.2.

4.2.1 Characteristics of the Modified ZIF-8

The FTIR spectra for ZIF-8-MeOH modified with bPEI (8-MeOH-45bPEI), produced a distinct peak at 3000-3400 cm^{-1} compared to that of the unmodified ZIF-8-MeOH as (Figure 33). This new peak is a hydroxyl group and could be attributed to the trapped MeOH in the ZIF-8.

Another new peak in the modified ZIF-8-MeOH spectrum appeared at 2900 cm^{-1}, which was likely related to the stretching of an -NH- bond. The peak at 2900 cm^{-1} is similar to the peak found in the FTIR spectrum of bPEI alone (Figure 34), and may increase in intensity if more bPEI is loaded on ZIF-8. According to (Prud'homme and Nabki 2020), bPEI exhibits NH modes at 3279 cm^{-1} and 2799 cm^{-1}. Therefore, the FTIR data indicate

that loading of bPEI into ZIF-8-MeOH was successful, but insufficient drying did not allow for further loading.

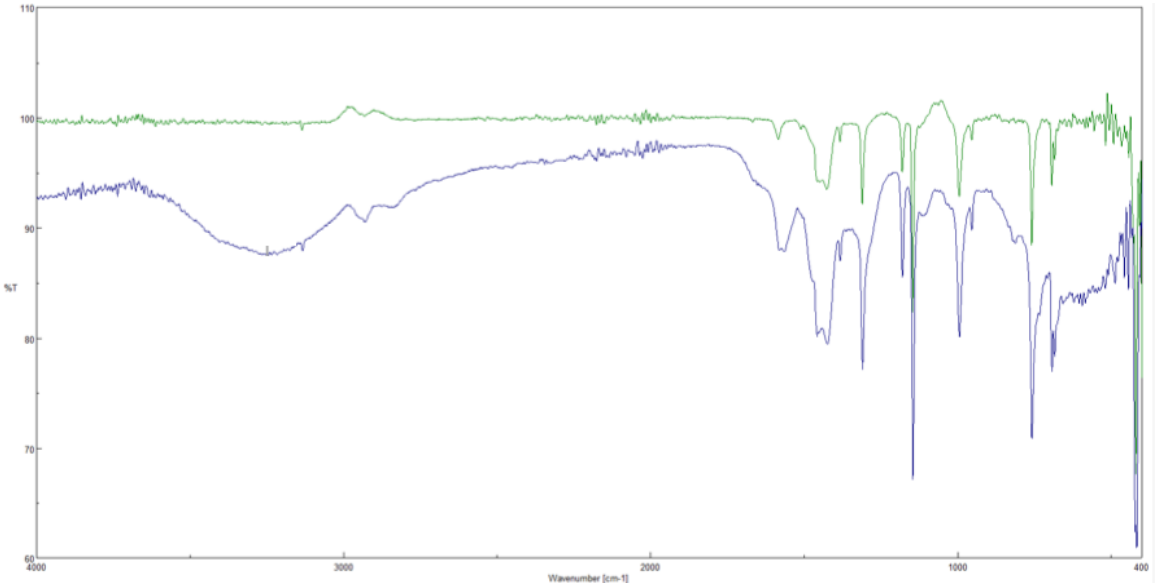

Figure 33. FTIR spectra of unmodified ZIF-8-MeOH (green) and modified ZIF-8-MeOH-45bPEI (blue)

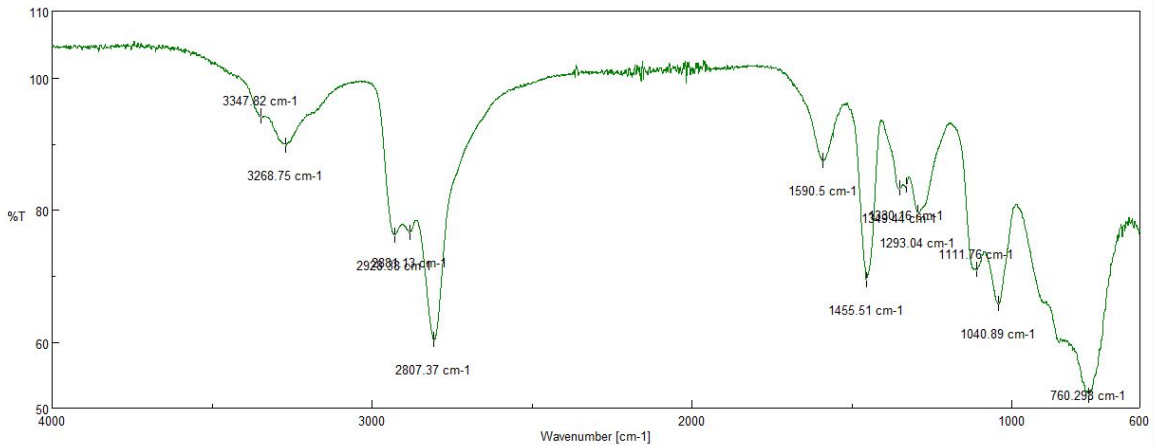

Figure 34. FTIR Spectra of bPEI

According to Xian et al. (2015), loading of LPEI produced a new peak, compared to the unmodified ZIF-8, in the range of 2550 and 3750 cm^{-1} (Figure 35). This peak was not likely caused by an –OH bond. It was rather attributed to LPEI as it was stronger as the

LPEI loading increased. The peak at 2838 cm^{-1} was due to stretching vibrations of a -NH- bond and increased with loading.

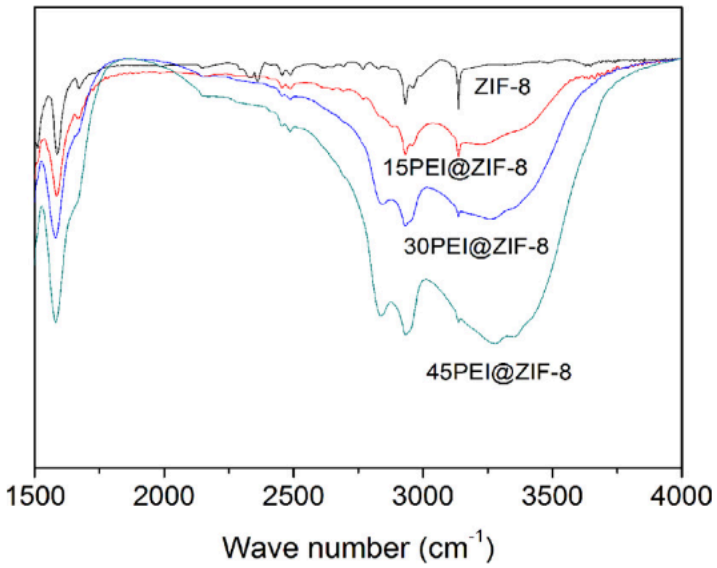

Figure 35. FTIR Spectra of unmodified ZIF-8 and ZIF-8 loaded with different percentages of LPEI (reproduced from (Xian et al. 2015)

TGA analysis was also performed to further confirm the successful loading of bPEI on ZIF-8-MeOH. The TGA results of the ZIF-8-MeOH-45bPEI are presented in Figure 36.. The weight of the sample decreased steadily with the increase in temperature from 400 K to 600 K (~126 to 330 ºC). On the other hand, the unmodified ZIF-8-MeOH did not start to decompose until the temperature reached ~700K (~450 ºC) as previously shown in Figure 30. These results further confirm that bPEI was successfully loaded into the ZIF-8-MeOH. However, the amount of bPEI loaded was low (~ 10%). It is noted that the initial increase at the beginning of the TGA profile may be due to N_2 adsorption while the consistent decline from 400K to 600 K and continued decline during the cooling stage of 600 K to 300 K indicate the loss of bPEI from the ZIF-8 sample.

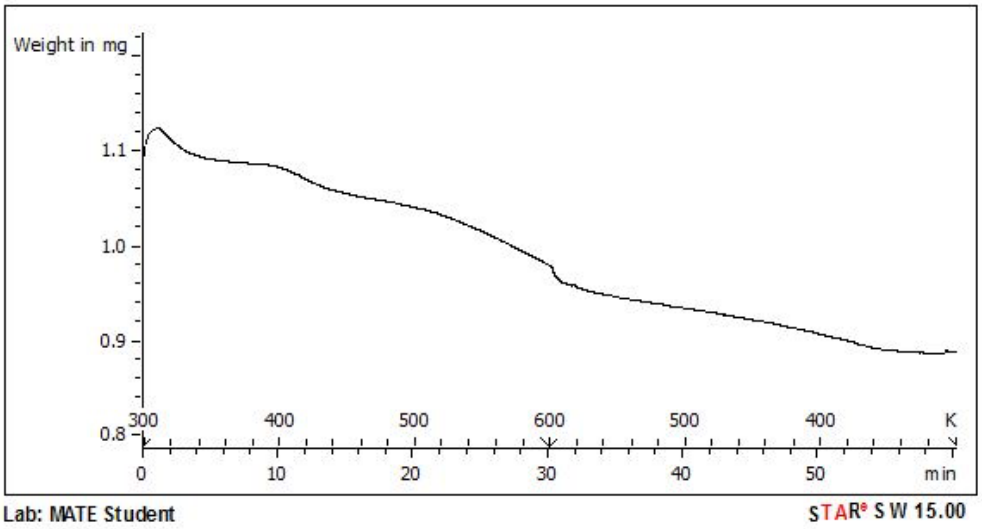

Figure 36. Experimental TGA results with ZIF-8-MeOH-45bPEI

The ZIF-8-DMF-45LPEI reported by Xian, et al. (2015) also exhibited similar decomposition trend to the one obtained in this study, with a gradual decline in weight from 400K to 850K, shown in Figure 37. These data show that LPEI loading of the ZIF-8-DMF was around 60% (w/w).

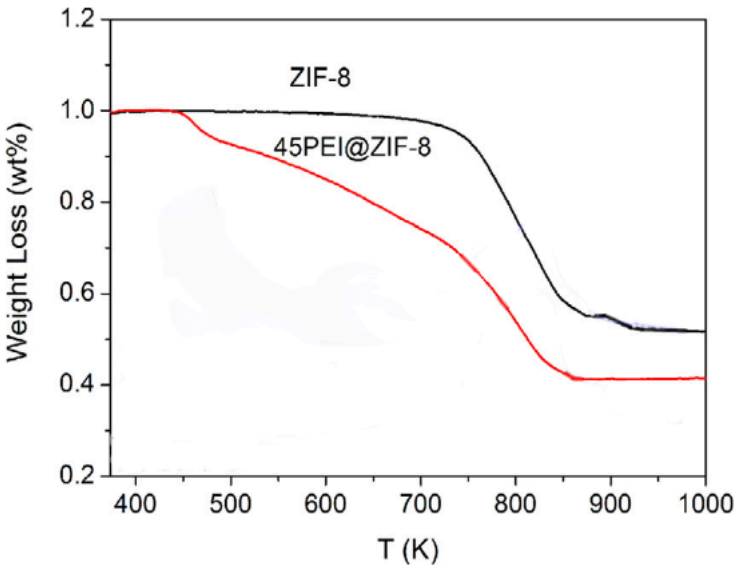

Figure 37. TGA data for ZIF-8-DMF & ZIF-8-DMF-45LPEI (reproduced from Xian et. al 2015)

A visual inspection of the modified and unmodified ZIF-8-MeOH samples was performed after placing the samples in an oven at 200°C (470 K) for 3 hours. The color of the unmodified ZIF-8-MeOH sample did not change while the modified sample exhibited an orange color resulting from the oxidation of bPEI (Figure 38). This visual observation is an additional confirmation of the successful modification of ZIF-8-MeOH with bPEI.

Figure 38. ZIF-8@bPEI heated at 200 ºC (473 K)

The XRD peaks of ZIF-8-MeOH-45bPEI are identical to those of the unmodified ZIF-8-MeOH as shown in Figure 39. This indicates that loading bPEI on ZIF-8 did not alter its crystalline structure and bPEI does not form a crystal of its own either. Xian et al. (2015) loaded ZIF-8-DMF with different amounts of linear PEI and their study showed that ZIF-8 maintained its crystal structure after loading with PEI as shown in Figure 40.

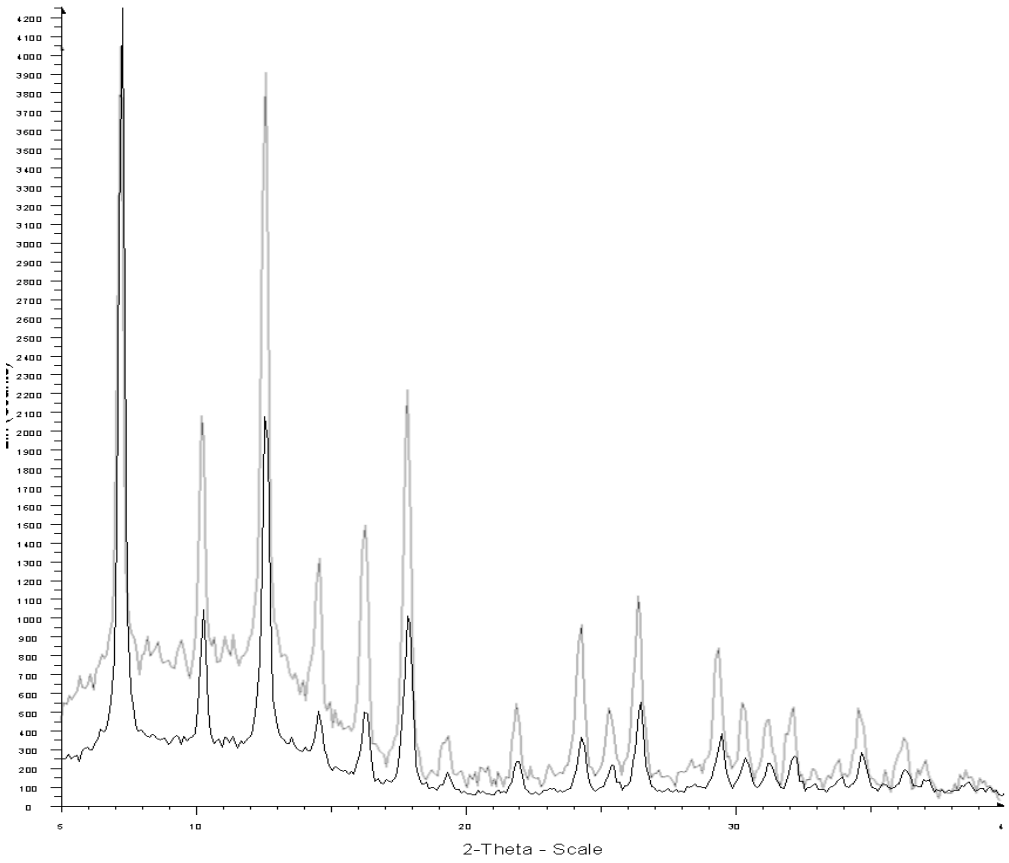

Figure 39. XRD of unmodified ZIF-8-MeOH (black) and modified ZIF-8-MeOH-45bPEI (gray)

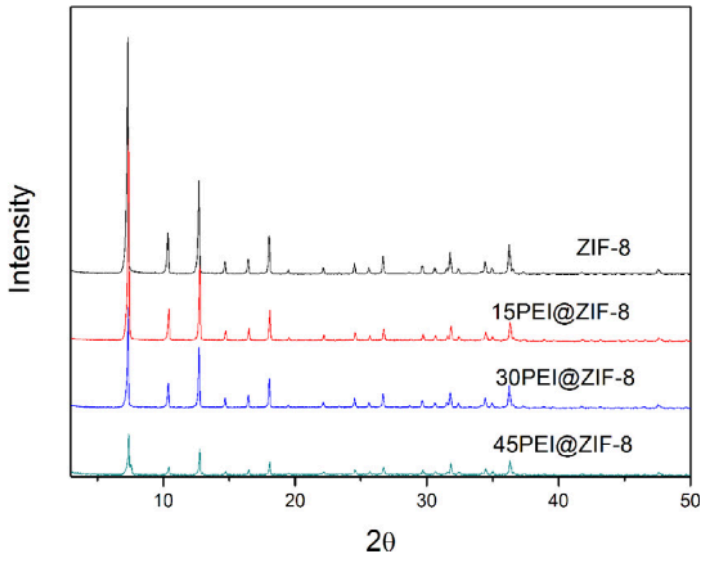

Figure 40. ZIF-8-DMF loaded with various loadings of linear PEI (reproduced from (Xian et al. 2015)

The BET analysis showed that ZIF-8-MeOH-45bPEI synthesized in this study had a surface area of 530 m^2/g, which is significantly lower than the surface area of 1300 m^2/g of the unmodified ZIF-8-MeOH. This reduction in surface area is another indicator that ZIF-8 was impregnated with bPEI.

Ta et al. (2018) reported that the ZIF-8-DMF45LPEI exhibited 21 m^2/g of surface area, which was substantially lower than their unmodified ZIF-8-DMF (1150 m^2/g). On the other hand, the surface area of the ZIF-8-MeOH-45bPEI produced in this study was 1300 m^2/g and was only reduced to 530 m^2/g after modification with bPEI. This surface area data coupled with the TGA data on the amount of bPEI loaded in ZIF-8 show that the loading levels achieved when LPEI was used by Ta et al. (2018) were much higher than the bPEI loading achieved in this study. The branching and the larger molecular weight of bPEI (MW = 1200) compared to the LPEI (MW = 300) were likely the reason for the insufficient bPEI loading. It was likely harder to impregnate a larger quantity of bPEI inside the ZIF-8 because bPEI molecules may have been blocked from reaching the smaller pores inside the ZIF-8 structure.

4.2.2 CO_2 and N_2 Adsorption Capacity of Modified ZIF-8

The results for CO_2 adsorption using ZIF-8-MeOH modified with two different loadings of bPEI are presented in Figure 41. There was an apparent increase in sorption capacity with the decrease in bPEI loading (Figure 41). However, this decrease is not statistically significant as the *p* value is > 0.05 at all pressure points tested.

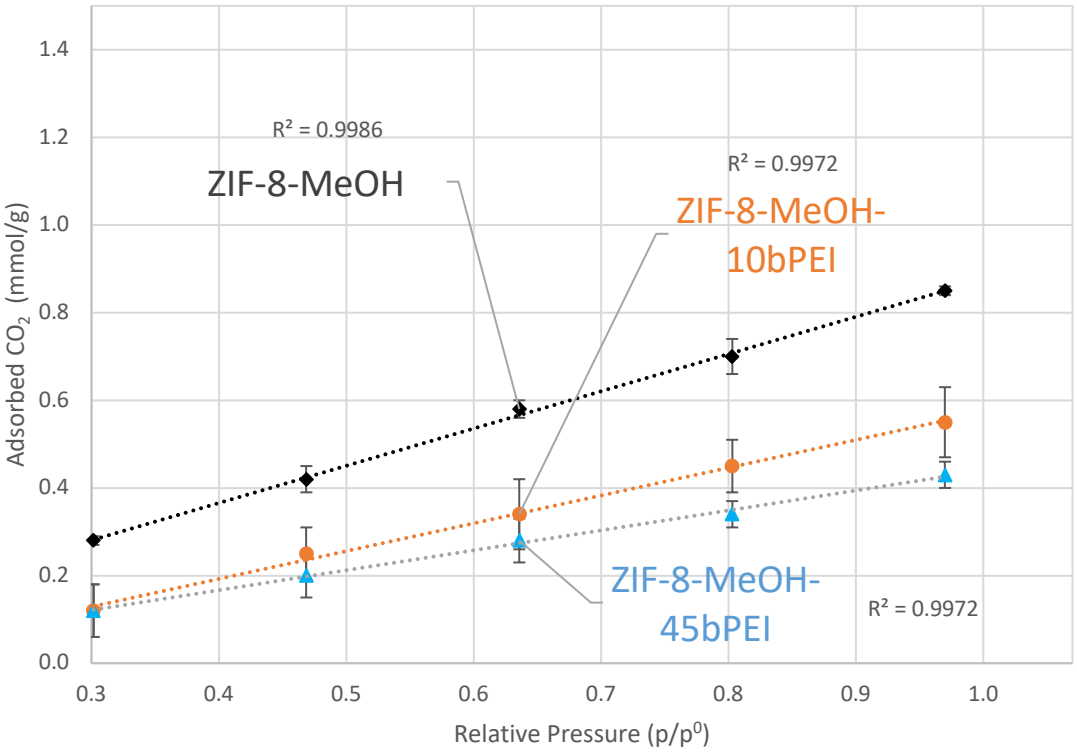

Figure 41. CO2 Adsorption Isotherms at 298K for ZIF-8-MeOH, ZIF-8-MeOH-10bPEI, and ZIF-8-MeOH-45bPEI [[graph says "series name"]]

The observed decrease is CO_2 sorption capacity when bPEI was loaded on ZIF-8-MeOH is not the desirable outcome. In addition, this reduction is not in agreement with the hypothesis stated earlier in this study that impregnating ZIF-8-MeOH with bPEI will result in a higher CO_2 adsorption capacity. Furthermore, the CO_2 sorption results obtained herein for the modified ZIF-8 are not in line with the studies published in the literature (Xian et al. 2015). For example, the study by Xian et al. (2015) showed that the ZIF-8-DMF loaded with different amounts of linear PEI exhibited an increase in CO_2 adsorption at higher LPEI loading, with ZIF-8-DMF-45LPEI adsorbing the most CO_2 at 1.3 mmol/g (Figure 42). This improvement in CO2 sorption capacity happened despite the fact that the surface area was reduced from 1150 m^2/g for the unmodified ZIF-8-DMF to only 21 m^2/g in the case of the modified ZIF-8-DMF-45LPEI. These results indicate that the

presence of PEI, which occupied a significant fraction of the pores of the ZIF-8, was more critical for CO_2 sorption than the availability of high surface area.

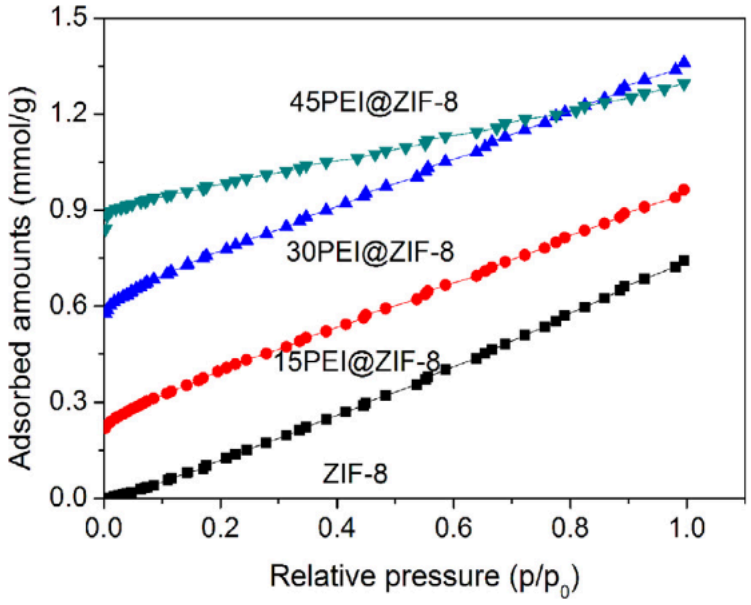

Figure 42. CO_2 adsorption isotherms for ZIF-8-DMF (ZIF-8) and different loadings of linear PEI at 298K (reproduced from Xian et. al 2015)

Possible explanations for the observed reduction in CO_2 sorption in this study when bPEI was loaded into ZIF-8-MeOH include: 1) branched PEI was not as effective as linear PEI for adsorbing CO_2, 2) longer experimental run times were needed for the bPEI to reach its sorption capacity, 3) insufficient amount of bPEI was loaded into the ZIF-8-MeOH to achieve a net increase in CO_2 sorption and compensate for the lost surface area occupied by the bPEI loaded into ZIF-8, and/or 4) ZIF-8 has trapped MeOH molecules after synthesis. The first explanation does not appear to be true, based on the information reported by (Zhao et al. 2012). They studied CO_2 sorption capacity of siliceous mesocellular foam particles loaded with linear as well as branched PEI molecules. Although linear PEI had a higher CO_2 adsorption capacity of 500 mg CO_2/g PEI, branched PEI also exhibited a relatively high sorption capacity of 382 mg CO_2/g PEI

in dry conditions (Zhao et al. 2012). Therefore, bPEI is an effective CO_2 sorbent and should have increased the adsorption capacity of the ZIF-8-MeOH in the current study.

The second explanation for the observed reduction in CO_2 after impregnation of ZIF-8-MEOH with bPEI is also highly unlikely. According to a study by (Prud'homme and Nabki 2020), a quartz crystal coated with bPEI took 20 minutes to reach adsorption capacity in an atmosphere of 0.01 partial pressure of CO_2. In the current study, longer run times were used for the modified ZIF-8 and the data were not recorded until the QCM reached equilibrium to ensure that no more CO_2 sorption was taking place.

The third explanation seems more likely for the observed reduction in CO_2 sorption by ZIF-8-MeOH-45bPEI. The TGA data showed that only about 10% of the mass of the modified ZIF sample was bPEI. This loading is significantly lower than, for example, the 60% value reported in the study by Ta et al. (2018) using linear PEI. Therefore, the sorption capacity added to the ZIF-8-MeOH through the impregnation with bPEI may have not been enough to overcome the loss in surface area of the modified ZIF-8-MeOH. As mentioned previously, the surface area of ZIF-8-MeOH decreased by ~ 60% (from 1300 to 530 m^2/g) after impregnation with bPEI. It is noted that CO_2 can be adsorbed on ZIF-8 by a combination of two mechanisms, physical adsorption on the surfaces of the pores of the ZIF-8 structure and chemical sorption to the PEI molecules. In the case of unmodified ZIF-8, surface area was the only factor that determined the sorption capacity of the ZIF-8. However, in the case of the modified ZIF-8 with a significant mass of linear PEI (Xian et al. 2015), the surface area played a minor role in determining the CO_2 sorption capacity of ZIF-8 compared to the amount of the modifier loaded on the ZIF-8. When the mass of the modifier was insignificant, like the case of this study, the surface area remained the governing factor for CO_2 sorption capacity of

the ZIF-8. Therefore, future research should investigate more effective ways to impregnate ZIF with bPEI.

The fourth reason of MeOH being trapped in the pores of ZIF-8 may also be plausible. This is supported by the results of the FTIR after modifying it with bPEI (Figure 33). The MeOH may have been trapped during synthesis or during impregnation. Weighing unmodified ZIF-8 before and after bake out may help determine whether MeOH did take up the pores and prevented more bPEI from being loaded onto ZIF-8.

4.3 Cost Analysis of ZIF-8 as a CO_2 Solid Sorbent Material

According to (DeSantis et al. 2017), the main cost of creating high quality MOFs is the solvent. To produce the ZIF-8 synthesized in this study, the costs include the price of Hmim, methanol, and $Zn(NO_3)_2 – 6H_2O$. Ta et. al (2018) indicated that only a 61.2% yield in reference to the metal salt is produced. With this assumption and cost data from Sigma-Aldrich, the cost for making 1 g of ZIF-8 is 0.89 cents. However, this cost could be singificantly lower when synthesis is scaled-up. For example, DeSantis et al. (2017) did a more thorough study on the cost of synthesis of Mg_2(dobdc) MOF and estimated a cost of $48.52 per kg of MOF. Assuming equal costs to produce ZIF-8 at large scale, the cost to remove one tonne of CO_2 could be about $11 million dollars. This cost can be further reduced depending on if the solvent is recycled, which was proven by (García-Palacín et al. 2020). To put this in perspective, the cost of CO_2 capture using amine scrubbing equated to $45 million per tonne of CO_2 removed for one plant (Wang et al. 2017). This shows that use of MOFs could be scaled up and utilized for CO_2 capture and be more cost effective than conventional amine scrubbing. It is important to note though that regeneration, maintenance, and energy costs for ZIF-8 were not considered in the study by DeSantis et. al (2017) and they can constitute a large fraction of the cost.

5. CONCLUSIONS, SYSTEM LIMITATIONS, AND FUTURE WORK

ZIF-8 was synthesized using water-based and methanol-based solvothermal methods. However, ZIF-8 made in water exhibited a substantially lower surface area compared to the ZIF-8 made in methanol and thus, its CO_2 sorption capacity was not tested. Adsorption experiments were conducted to measure the sorption capacity of the ZIF-8 made by methanol at pressures ranging from 0.3 – 1 bar to simulate pressures of CO_2 representative of flue gases.

The ZIF-8 made in methanol (ZIF-8-MeOH) had a CO_2 sorption capacity that was comparable to that of ZIF-8 made using DMF (ZIF-8-DMF) by Xian et al. (2015) at all gas pressures tested. The XRD data showed that the crystal structure of the ZIF-8-MeOH was similar to that of the ZIF-8-DMF. Furthermore, the surface area analysis showed that the ZIF-8-MeOH had a slightly higher surface area compared to that of ZIF-8-DMF. These results show that the more eco-friendly ZIF-8 tested in this study is a good solid sorbent candidate that can replace ZIF-8-DMF for carbon capture applications.

The ZIF-8-MeOH was modified using branched polyethyleneimine (bPEI) with the goal to enhance its sorption capacity. The FTIR and TGA characterization results indicated that bPEI was successfully loaded onto the ZIF-8-MeOH. However, the bPEI loading was about 10% by weight, which was likely not sufficient to enhance the performance and resulted in lowering the sorption capacity by reducing the surface area of the ZIF-8-MeOH. This reduction in surface area caused a tangible decrease in CO_2 sorption compared to the unmodified ZIF-8-MeOH.

5.1 Limitations of the Experimental Setup

Due to budget constraints and equipment limitations, the samples were only tested at pressures of 0.34 bar, 0.51 bar, 0.67 bar, 0.84 bar, and 1 bar (20, 15, 10, 5, and 0 in Hg)

for the isotherms. Purchasing a vacuum pump that could reach close to 0.1 bar (1 in Hg) would allow for testing lower pressures. Lower pressures of 0.1 bar are needed because the partial pressure of CO_2 in flue gas is typically around 0.15 bar.

The QCM system assembled and used in this study was set up to have a precision of ± 1 Hz of frequency change. However, this precision needs to be improved to ± 0.01 Hz of change to improve the sensitivity and accuracy when N_2 adsorption testing is performed. This is needed for future experiments to evaluate CO_2 selectivity of the ZIFs. The QCM system used herein has the capability to achieve this precision as per the manufacturer information, but unwanted frequency shifts need to be accounted for. Frequency shifts can occur due to small temperature fluctuations. Use of a heating tape for the gas hoses as well as a heating mantle can allow for fewer frequency shifts due to temperature. Along with this, vacuum leaks in the system can affect the frequency readings and use of vacuum rating fittings, KF fittings, can remedy this problem. Installation of mass flowmeters as well could also allow for a better control of the amount of gas entering the system because too much gas entering at once can cause large fluctuations in frequency.

The drop-casting technique used in this study was not the optimal method to load the ZIF-8 samples on the QCM crystals because it results in uneven coating on the crystal surface as shown in Figure 43. A great deal of trial and error was done to balance a sufficient amount of sample to coat the crystal while not causing it to fail. If too much sample is loaded onto the crystal, the stress caused by the mass causes the crystal to stop oscillating. This drop-casting technique also may add to the uncertainty of measurements due to crystal holder partially covering the crystal and so the outer diameter is not utilized. These problems indicate a need for a better coating technique in future studies such as spin coating.

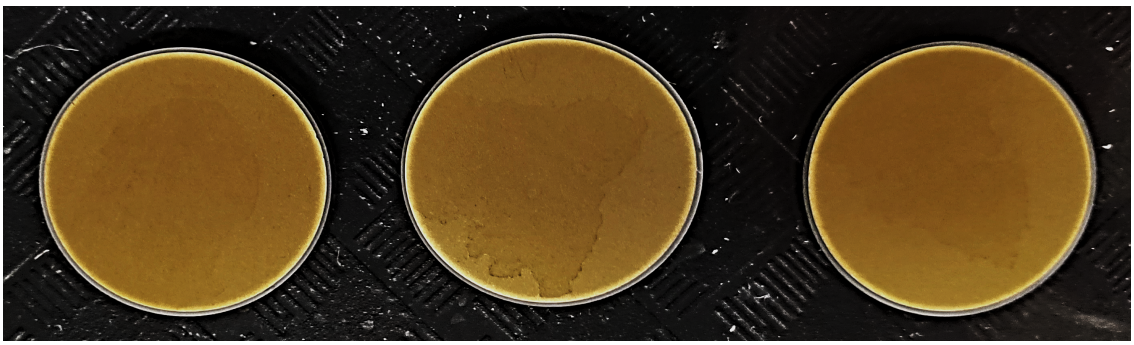

Figure 43. Uneven coating due to drop-casting technique

To increase the ease of experiments, the installation of a pressure transducer and solenoid valve should be considered. If the system is retrofitted with KF fittings to become leak proof, the use of the transducer and solenoid valve can help automate the pressure steps for the experiments and thus allow for greater efficiency. It is highly recommended to install a relief valve on the QCM setup to allow for use of ambient air instead of nitrogen or carbon dioxide gas to bring the system back up to atmospheric pressure. Lastly, the installation of a larger diameter hose to the vacuum pump should be performed to allow for efficient and safe pumping because the pump sometimes shuts off automatically due to the small volume of the current hose.

5.2 Future Work

5.2.1 Investigate methods to load higher bPEI amounts into ZIF-8-MeOH

According to (Aarti et al. 2016), Cu-BTC, another MOF, had an increase in CO_2 adsorption capacity when it was modified with a bPEI. Although ZIF-8 is an entirely different structure than MOF Cu-BTC, these results show that bPEI has potential if a method can be developed to sufficiently load it into ZIF-8-MeOH. Suggestions for modifications to the bPEI impregnation method include using longer reaction times and dissolving less bPEI in the solvent to make a less viscous solution, which may enhance the diffusivity of bPEI molecules into the ZIF-8 porous structure. Characterization of the pore volume of ZIF-8-MeOH before and after modification with bPEI can provide insights

on ways to enhance the impregnation process of ZIF-8-MeOH with bPEI. Another method of loading could utilize grafting rather than physical impregnation as reported by (Gao et al. 2018). Gao et. al (2018) reported an increase in surface area, pore volume, and micropore diameters rather than a decrease as seen with physical impregnation.

5.2.2 Explore other molar weight variants of linear PEI and branched PEI

Impregnation of ZIF-8-MeOH with a low to high range of molecular weights (300 - 800) of linear PEI should be performed, and the CO_2 sorption capacity of these modified ZIF-8-MeOH particles should be tested. (Goeppert et al. 2014) showed that linear PEI with a molar weight of 800 resulted in the highest CO_2 adsorption capacity for fumed silica at 50% loading. Other molar weights of bPEI should also be investigated, specifically a MW of 800, which was used in the modification of NU-1000, another type of MOF (Kang et al. 2019). Use of other amine groups for functionalization of ZIF-8-MeOH may be possible but should be tested for leaching after functionalization of MOFs. Ethylenimines and other amine groups of low molar weight (<600) have been shown to leach and volatilize from solid sorbents, leading to lower CO_2 adsorption capacity (Goeppert et al. 2014).

5.2.3 Explore other hydrophobic MOFs

One of the main reasons ZIF-8 was chosen in this study was because of its high selectivity and hydrophobicity. Other hydrophobic MOFs such as superhydrophobic ZIF-67, UPC-21, and superhydrophobic ZIF-90 could be investigated with the amine groups mentioned before (Antwi-Baah and Liu 2018). Use of the eco-friendly cyclodextrin metal organic frameworks is also recommended due to its hydrophobic internal cavity (Yao et. al 2018).

5.2.4 Selectivity tests for CO_2/N_2 and CO_2/H_2O and temperature trials

If the recommendations mentioned above lead to increase in CO_2 adsorption capacities, tests should be conducted to determine the selectivity of MOFs to CO_2 in the presence

of nitrogen and water vapor. These tests are essential to evaluate how the developed MOFs would perform under representative flue gas conditions. Testing the performance of the MOFs under a range of different temperatures is needed because previous research showed that linear PEI has increased CO_2 sorption capacity of ZIF-8-DMF at higher temperatures (Xian et al. 2015) while branched PEI resulted in a decrease is sorption capacity of Cu-BTC (Aarti et al. 2016).

5.2.5 Recyclability and Sustainability

A techno-economic analysis performed on four MOFs: MOF-5, HKUST-1, Ni_2(dobdc) and Mg_2(dobdc) using three different synthesis methods (DeSantis et al. 2017). This analysis showed that the liquid assisted grinding (LAG) method, as well as the aqueous method, were the most scalable (DeSantis, et.al, 2017). The LAG method incorporates solids and a low amount of solvent in a high attrition mill to produce MOFs at a low cost (DeSantis et. al, 2017). One the other hand, the aqueous method is similar to the solvothermal method used herein but the reaction is held under reflux. The leading costs in creating MOFs is the large amount of solvents used and can account for 40-79% of the cost of the MOFs (DeSantis et. al, 2017). Only by recycling greater than 90% of the solvent can the solvothermal method be comparable to the other low cost methods (DeSantis et.al, 2017). Future work should investigate the feasibility of reusing the solvent waste resulting from synthesis of ZIF-8 to produce new batches of ZIF-8 as demonstrated by García-Palacín, et al. (2020). This can increase the yield and make a more sustainable ZIF-8 for use in carbon capture applications.

BIBLIOGRAPHY

Aarti et al. 2016. “-Polyethyleneimine: An Efficient MOF Composite for Effective CO2 Separation.” *RSC Advances* 6(95): 93003–9.

Alassi, Abdulrahman, Mohieddine Benammar, and Dan Brett. 2017. “Quartz Crystal Microbalance Electronic Interfacing Systems: A Review.” *Sensors (Switzerland)* 17(12).

Alothman, Zeid A. 2012. “A Review: Fundamental Aspects of Silicate Mesoporous Materials.” *Materials* 5(12): 2874–2902.

Antwi-Baah, Ruth, and Heyang Liu. 2018. “Recent Hydrophobic Metal-Organic Frameworks and Their Applications.” *Materials* 11(11).

Changing Role of Natural Gas in Energy Generation.

Chen, Binling, Zhuxian Yang, Yanqiu Zhu, and Yongde Xia. 2014. *Zeolitic Imidazolate Framework Materials: Recent Progress in Synthesis and Applications*. www.rsc.org/materialsA.

Chung, Yongchul G. et al. 2019. “Advances, Updates, and Analytics for the Computation-Ready, Experimental Metal-Organic Framework Database: CoRE MOF 2019.” *Journal of Chemical and Engineering Data* 64(12): 5985–98.

DeSantis, Daniel et al. 2017. “Techno-Economic Analysis of Metal-Organic Frameworks for Hydrogen and Natural Gas Storage.” *Energy and Fuels* 31(2): 2024–32.

Ding, Meili, Robinson Flaig, Hai-Long Jiang, and Omar Yaghi. 2018. “Carbon Capture and Conversion Using Metal-Organic Frameworks and MOF-Based Materials.” *Journal of Materials Chemistry B* 6(35).

Dutcher, Bryce, Maohong Fan, and Armistead G. Russell. 2015. “Amine-Based CO2 Capture Technology Development from the Beginning of 2013-A Review.” *ACS Applied Materials and Interfaces* 7(4): 2137–48.

Energy Agency, International. 2018. *Global Energy & CO2 Status Report: The Latest Trends in Energy and Emissions in 2018*. www.iea.org/t&c/.

Gao, Yongqiang et al. 2018. “In Situ Synthesis of Polymer Grafted ZIFs and Application in Mixed Matrix Membrane for CO2 Separation.” *Journal of Materials Chemistry A* 6(7): 3151–61.

García-Palacín, Marta et al. 2020. “Sized-Controlled ZIF-8 Nanoparticle Synthesis from Recycled Mother Liquors: Environmental Impact Assessment.” *ACS Sustainable Chemistry and Engineering* 8(7): 2973–80.

Ghanbari, Taravat, Faisal Abnisa, and Wan Mohd Ashri Wan Daud. 2020. “A Review on Production of Metal Organic Frameworks (MOF) for CO2 Adsorption.” *Science of the Total Environment* 707.

Goeppert, Alain et al. 2014. “Easily Regenerable Solid Adsorbents Based on Polyamines for Carbon Dioxide Capture from the Air.” *ChemSusChem* 7(5): 1386–97.

Hesketh, Peter, Sankar Nair, and Todd Sulchek. *QUARTZ CRYSTAL MICROBALANCE ADSORPTION APPARATUS FOR HIGH PRESSURE GAS ADSORPTION MEASUREMENTS IN NANOMATERIALS*.

Hoegh-Guldberg, O. et al. 2019. “The Human Imperative of Stabilizing Global Climate Change at 1.5°C.” *Science* 365(6459).

Jansen, Daniel et al. 2015. “Pre-Combustion CO2 Capture.” *International Journal of Greenhouse Gas Control* 40: 167–87.

Joshi, Dirgha Raj, and Nisha Adhikari. 2019. “An Overview on Common Organic Solvents and Their Toxicity.” *Journal of Pharmaceutical Research International*: 1–18.

Kang, Jo Hong et al. 2019. “Extraordinarily Selective Adsorption of CO2 over N2 in a Polyethyleneimine-Impregnated NU-1000 Material.” *Microporous and Mesoporous Materials* 281: 84–91.

Kanniche, Mohamed et al. 2010. “Pre-Combustion, Post-Combustion and Oxy-Combustion in Thermal Power Plant for CO2 Capture.” *Applied Thermal Engineering* 30(1): 53–62.

Kashan, Mohammad Ali Mohammadzadeh et al. 2017. “QCM Coupled Resonating Systems Under Vacuum: Sensitivity and Characteristics.” *IEEE Sensors Journal* 17(16): 5044–49.

Koytsoumpa, Efthymia Ioanna, Christian Bergins, and Emmanouil Kakaras. 2018. “The CO2 Economy: Review of CO2 Capture and Reuse Technologies.” *Journal of Supercritical Fluids* 132: 3–16.

Lee, Yu Ri et al. 2015. “ZIF-8: A Comparison of Synthesis Methods.” *Chemical Engineering Journal* 271: 276–80.

Masson-Delmotte, Valérie et al. 2019. *Global Warming of 1.5°C An IPCC Special Report on the Impacts of Global Warming of 1.5°C above Pre-Industrial Levels and Related Global Greenhouse Gas Emission Pathways, in the Context of Strengthening the Global Response to the Threat of Climate Change, Sustainable Development, and Efforts to Eradicate Poverty Edited by Science Officer Science Assistant Graphics Officer Working Group I Technical Support Unit*. www.environmentalgraphiti.org.

Park, Kyo Sung et al. 2006. *Exceptional Chemical and Thermal Stability of Zeolitic Imidazolate Frameworks*. www.pnas.orgcgidoi10.1073pnas.0602439103.

Phan, Anh et al. 2010. “Synthesis, Structure, and Carbon Dioxide Capture Properties of Zeolitic Imidazolate Frameworks.” *Accounts of Chemical Research* 43(1): 58–67.

Prud’homme, Alberto, and Frederic Nabki. 2020. “Comparison between Linear and Branched Polyethylenimine and Reduced Graphene Oxide Coatings as a Capture Layer for Micro Resonant CO2 Gas Concentration Sensors.” *Sensors (Switzerland)* 20(7).

Rochelle, G. T. 2016. “Conventional Amine Scrubbing for CO2 Capture.” In *Absorption-Based Post-Combustion Capture of Carbon Dioxide*, Elsevier Inc., 35–67.

Safaei, Mohadeseh et al. 2019. “A Review on Metal-Organic Frameworks: Synthesis and Applications.” *TrAC - Trends in Analytical Chemistry* 118: 401–25.

Samanta, Arunkumar et al. 2012. “Post-Combustion CO 2 Capture Using Solid Sorbents: A Review.” *Industrial and Engineering Chemistry Research* 51(4): 1438–63.

Sanz-Pérez, Eloy S., Christopher R. Murdock, Stephanie A. Didas, and Christopher W. Jones. 2016. “Direct Capture of CO2 from Ambient Air.” *Chemical Reviews* 116(19): 11840–76.

Sarango, Lilian et al. 2018. “Homogeneous Thin Coatings of Zeolitic Imidazolate Frameworks Prepared on Quartz Crystal Sensors for CO2 Adsorption.” *Microporous and Mesoporous Materials* 272: 44–52.

Sneddon, Gregor, Alex Greenaway, and Humphrey H.P. Yiu. 2014. “The Potential Applications of Nanoporous Materials for the Adsorption, Separation, and Catalytic Conversion of Carbon Dioxide.” *Advanced Energy Materials* 4(10).

Songolzadeh, Mohammad, Mansooreh Soleimani, Maryam Takht Ravanchi, and Reza Songolzadeh. 2014. “Carbon Dioxide Separation from Flue Gases: A Technological Review Emphasizing Reduction in Greenhouse Gas Emissions.” *The Scientific World Journal* 2014.

Ta, Don N. et al. 2018. “Preparation of Nano-ZIF-8 in Methanol with High Yield.” *Canadian Journal of Chemical Engineering* 96(7): 1518–31.

Tsionsky, V, L Daikhin, M Urbakh, and E Gileadi. 1995. 11 Langmuir *Behavior of Quartz Crystal Microbalance in Nonadsorbed Gases at High Pressures*.

Wang, Yuan et al. 2017. “A Review of Post-Combustion CO2 Capture Technologies from Coal-Fired Power Plants.” In *Energy Procedia*, Elsevier Ltd, 650–65.

Wilmer, Christopher E. et al. 2012. “Large-Scale Screening of Hypothetical Metal-Organic Frameworks.” *Nature Chemistry* 4(2): 83–89.

Wu, You Ting et al. 2004. “Quartz Crystal Microbalance (QCM) in High-Pressure Carbon Dioxide (CO 2): Experimental Aspects of QCM Theory and CO 2 Adsorption.” *Langmuir* 20(9): 3665–73.

Xian, Shikai et al. 2015. “Vapor-Enhanced CO2 Adsorption Mechanism of Composite PEI@ZIF-8 Modified by Polyethyleneimine for CO2/N2 Separation.” *Chemical Engineering Journal* 280: 363–69.

Zhang, Zhijuan et al. 2013. “Enhancement of CO2 Adsorption and CO2/N2 Selectivity on ZIF-8 via Postsynthetic Modification.” *AIChE Journal* 59(6): 2195–2206.

Zhao, Junqi et al. 2012. “Polyethylenimine-Impregnated Siliceous Mesocellular Foam Particles as High Capacity CO2 Adsorbents.” *RSC Advances* 2(16): 6509–19.